Spectrochimica Acta Part A: Molecular and Biomolecular Spectroscopy 258 (2021) 119868

Contents lists available at ScienceDirect

Spectrochimica Acta Part A: Molecular and Biomolecular Spectroscopy

journal homepage: www.elsevier.com/locate/saa

Dual–channel colorimetric fluorescent probe for determination of hydrazine and mercury ion

Xiaofeng Yang *, Yiming Ding, Yexin Li, Mei Yan, Yu Cui, Guoxin Sun

School of Chemistry and Chemical Engineering, University of Jinan, No. 336, West Road of Nan Xinzhuang, Jinan 250022, Shandong, China

HIGHLIGHTS

- A multifunctional colorimetric and fluorescent probe PI-Rh has been developed.
- Discriminative detection of hydrazine and mercury ion with differential colorimetric and fluorescence outputs.
- High sensitivity, superior selectivity, and low detection limit for hydrazine and mercury ion.
- Its superiority in practical applications to sense hydrazine and mercury ion.

GRAPHICAL ABSTRACT

ARTICLE INFO

Article history:
Received 21 November 2020
Received in revised form 4 April 2021
Accepted 21 April 2021
Available online 24 April 2021

Keywords:
Chemosensor
Hydrazine
Mercury ion
Discriminative
Practicality

ABSTRACT

Hydrazine and mercury (Hg) poisoning represented a serious hazard to human health. So, developing method to detect and recognize them is highly desirable. Here, we prepared a multifunctional colorimetric and fluorescent probe (**PI-Rh**) consisting of a phenanthroimidazole (**PI**) dye conjugated with a Rhodamine (**Rh**) group for the effective recognition of hydrazine and Hg^{2+}, induvidually and collectively, with different colorimetric and fluorescence outputs. Probe **PI-Rh** displays low detection limits measured to be 0.0632 μM (~2 ppb) and 0.0101 μM (~2 ppb) respectively for hydrazine and Hg^{2+} with high selectivity and excellent sensitivity. Moreover, the experimental results indicated that the superiority of this probe lied in its wide applications, for example, successful response in real water, and soil analysis. Interestingly, an visual, rapid, and real–time detection of gaseous hydrazine can be realized with 0.2793 μM detection limit using the facile **PI-Rh**–impregnated test paper.

1. Introduction

Hydrazine (N_2H_4) is flammable and explosive, and is usually served as a propellant in rocket propulsion systems and missiles [1]. It is also a strong reducing agent, which can remove oxygen in the thermal circulation system and achieve the effect of inhibiting metal corrosion [2]. In addition, it is also an important chemical reagent in chemical industry [3], pharmaceutical industry [4] and pesticide industry [5]. However, research suggested that hydrazine and its aqueous solutions have great toxicity to humans and animals [6], and could cause adverse effects on liver, kidney, lung, central nervous system, respiratory tract and other systems [7,8]. Recently, the U.S. Environmental Protection Agency (EPA) identified hydrazine as a potential carcinogen, and the threshold limit value (TLV) for hydrazine in drinking water was recommended to be as low as 10 ppb [9]. Therefore, it is of great significance to develop an effective method to detect trace hydrazine hydrate.

Several traditional analytical methods for hydrazine detection are chromatography [10–13], electrochemistry [14,15], titrimetry [16,17], surface-enhanced Raman spectroscopy [18], and colorimetric-/fluorometric-analysis [19–63]. Among them,

* Corresponding authors.
E-mail address: chm_yangxf@ujn.edu.cn (X. Yang).

https://doi.org/10.1016/j.saa.2021.119868
1386-1425/

fluorescence detection has attracted much attention owing to its high efficiency, real-time, on-line analysis and simplicity. Hydrazine, as a strong nucleophilic reagent, could selectively react with some structure of functional groups, such as aromatic aldehydes [19–21], malononitrile [22–31], ethyl cyanoacetate [32], ester [33–50], phthalimide [51–58], trifluoroacetylacetonate [59], conjugated-1,3-diketo [60], chalcone [61,62]. Inspired by the special nucleophilic characteristics of hydrazine, herein, we conceived a new compound **PI-Rh** based on a nonfluorescent Rhodamine (**Rh**) with ethylene diamine as a linker with phenanthroimidazole (**PI**) benzaldehyde (Scheme 1**A**). This work confirmed that hydrazine could react with the imine bond of compound **PI-Rh** resulting in yellow–green fluorescence blue-shifting cyan fluorescence. The hydrogen bond fromed between the compound **PI-Rh** and hydrazine played a very important role in such response strategy, therefore, this probe should expect to work well without disruption from other nucleophile reagents except for hydroxylamine. Its sensing property and response mechanism were investigated in detailed. All analysis and application results showed that not only the aqueous solution of **PI-Rh** could used as an effective probe for detetion hydrazine in pure water, real water samples and in soil, but also **PI-Rh** was successfully fabricated into paper-based test stripes for visual, rapid, sensitive, and real-time detection of gaseous hydrazine with a low detection limit.

Mercury (Hg) is widely used in metallurgy, instrument and lamp manufacturing, however, its opening and smelting processes often cause environmental pollution. Organic mercury and inorganic mercury are formed after the oxidation of metal mercury, and some of them will enter the human body through the enrichment of food chain [64]. The most horrible thing is that accumulation of mercury ions (Hg^{2+}) could damage the central nervous system in organisms and cause various cognitive, kidney failure, brain damage, and motor disorders [65]. Therefore, it is very important to detect the mercury concentration in clinical diagnosis and environment quickly and efficiently. In recent years, a large number of fluorescent probes based on ring-opening of spirocyclic xanthene and related derivatives for detection Hg^{2+} have been developed [66–80]. However, such type probes would be commonly interfered by other competing metal ions and no satisfactory selectivity would be obtained. To overcome these obstacles, some novel reaction-based sensing strategies relying on a specific chemical reaction to Hg^{2+} have been developed, such as a specific Hg^{2+}-promoted cyclization of an aryl vinyl ether [81–85] and the desulfurization reaction promoted by Hg^{2+} (including the elimination reaction [86,87], the hydrolysis [88–93], ring opening reaction [94]). Although great progresses have been achieved in this regard, it is still significant to design new probes with high efficiency for Hg^{2+} detection.

Herein, we pregnanted with a new "reactive" probe **PI-Rh** for response to Hg^{2+} (Scheme 1**B**). We proposed that **PI-Rh** based on the hydrolysis of an imine group was specifically promoted by Hg^{2+}. Additionally, the proposed hydrolysates were compound **PI-1** that possessed two different emission channels (blue and green lights), and compound **Rh-2** that possessed a red fluorescene (Fig. 1**B**). Thus, the imine group of probe **PI-Rh** was expected to undergo a Hg^{2+}-promoted hydrolysis to produce the final mixture of aldehye **PI-1** and Rhodamine B derivative **Rh-2**, which emited an approximate organic white fluorescence with three different channels, blue, green and red. As expected, probe **PI-Rh** could be applied to effectively detect Hg^{2+} in both colorimetric and ratiometric mode. Moreover, it could be successfully used for analyzing Hg^{2+} in real water samples, and the facile **PI-Rh**-impregnated test paper could be also developed as an effective method of naked-eye detection of mercury ion.

2. Results and discussion

2.1. Design strategy of the compound *PI-Rh*

The synthetic routes of compound **PI-Rh**, the **PI** derivatives (**PI-0**, **PI-1**, and **PI-2**), and the **Rh** derivatives (**Rh-1** and **Rh-2**) were illustrated in Scheme 2. Compounds **PI-0** and **PI-1** were prepared according to our group's previous work [95]. Compound **PI-2** was synthesized by a simple condensation of compound **PI-1** and hydrazine hydrate. Compound **Rh-1** was prepared according to previous work [75]. Compound **Rh-1** had undergone the $HgCl_2$-promoted nucleophilic addition by H_2O to generate **Rh-2**. Finally,

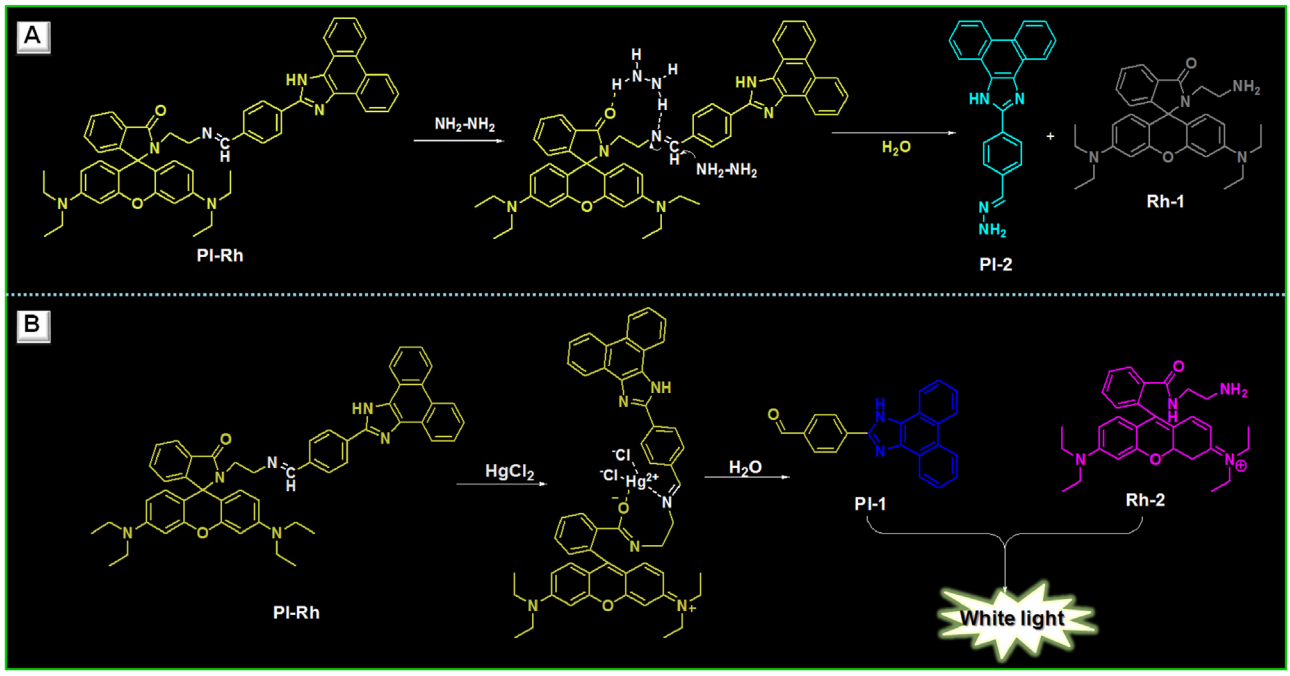

Scheme 1. Design and sensing mechanism of the new hydrazine and Hg^{2+} probe **PI-Rh**.

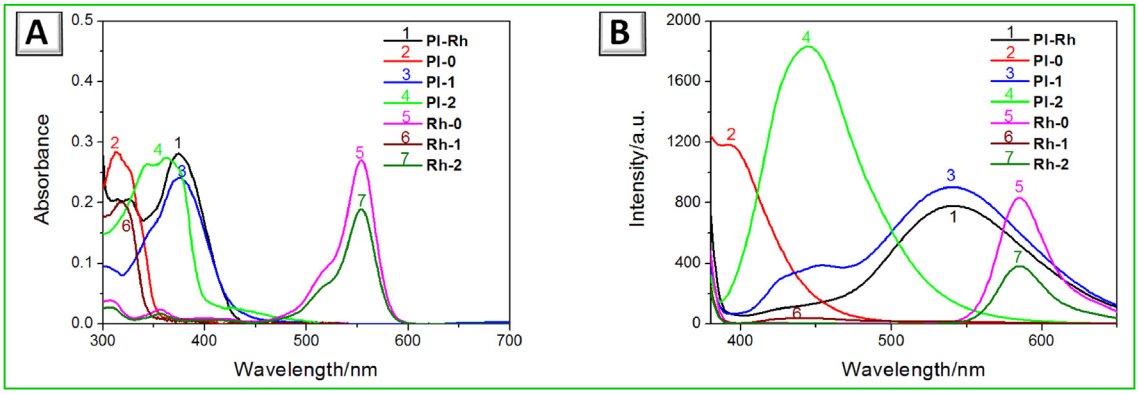

Fig. 1. UV–vis absorption (**A**) and emission spectra (**B**) of compound **PI-Rh** (10 μM), **PI-0** (10 μM), **PI-1** (10 μM), **PI-2** (10 μM), **Rh-0** (10 μM), **Rh-1**(10 μM), and **Rh-2** (10 μM) in DMSO–PBS buffer (2:8, v/v, pH 7.4) solution, respectively. Excitation wavelength: 370 nm.

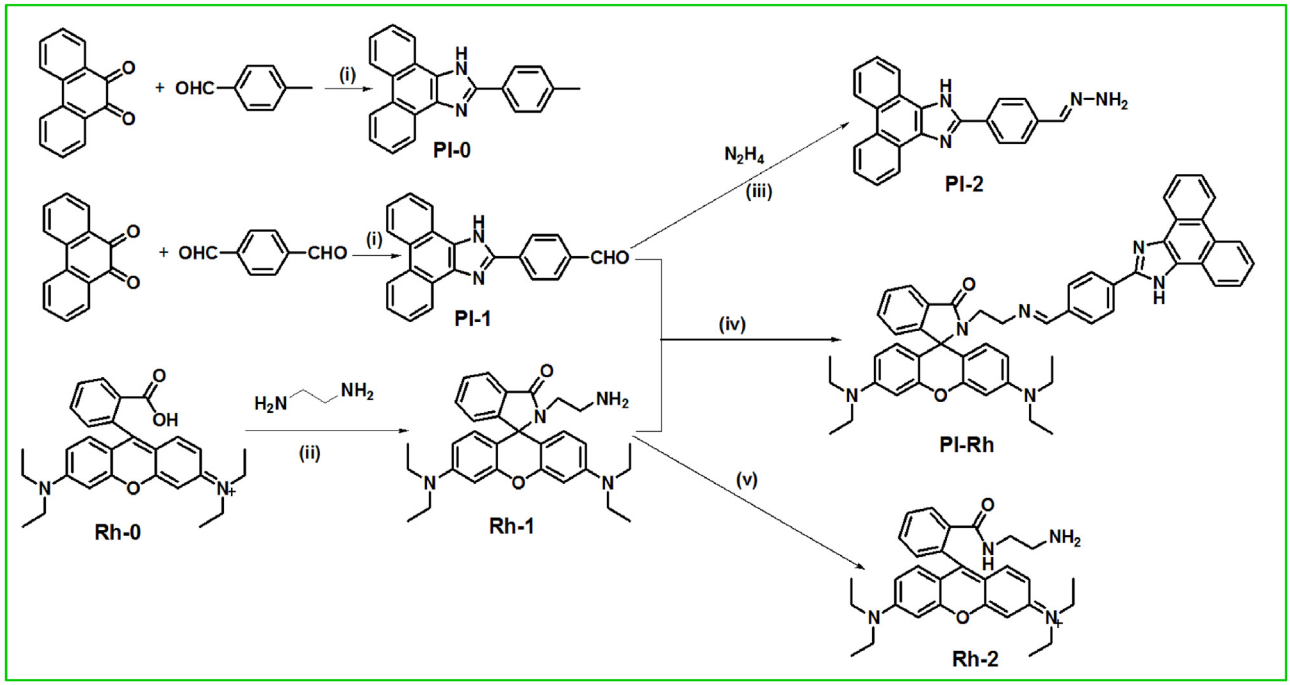

Scheme 2. Synthetic routes for compounds **PI-0**, **PI-1**, **PI-2**, **Rh-1**, **Rh-2** and **PI-Rh**, (i) CH_3COONH_4, CH_3COOH, 100 °C, 1 h; (ii) EtOH, reflux, 12 h; (iii) EtOH–DMF, r.t., 4 h; (iv) DMF, reflux, 12 h; (v) $HgCl_2$, DMSO–d_6/D_2O, r.t.

the target compound **PI-Rh** was easily synthesized by condensation of compounds **PI-1** and **Rh-1** in refluxed DMF solution. The chemical structures of these compounds were confirmed with ^1H NMR, ^{13}C NMR, and high resolution mass spectroscopy (HRMS). Corresponding analytical characterization data were provided in the supporting information.

Multifunctional fluorescent probe **PI-Rh** we designed was based on the following considerations: a **PI** fluorophore was chosen because its absorption and emission spectra were completely separated (Fig. 1), and its large Stokes shift could remove the endogenous autofluorescence interference satisfactorily [96]. The first reason we selected Rhodamine B as the other fluorophore was that the hydrogen bonds formed between the spirolactam of **PI-Rh** and hydrazine could activate imine unit to improve its electrophilic ability, and favor for the next chemoslective nucleophilic addition and the subsequent hydrolysable of the imine linkage as shown in Scheme 1. Thus, compound **PI-Rh** could be used as a new ratiometric probe for fluorescence detection of hydrazine. The second reason we selected Rhodamine B as the other fluorophore was that the binding of the $HgCl_2$ with compound **PI-Rh** could induce the ring-opening of the spirocyclic **PI-Rh**, and promote the hydrolysis of the imine group produce the corresponding mixture of aldehye **PI-1** and Rhodamine B derivative **Rh-2** with an approximate organic white fluorescenceas shown in Scheme 2.

2.2. Spectroscopic analysis

2.2.1. Photophysical characterization of *PI-Rh*

With these compounds in hand, we began to study their optical properties in DMSO–PBS buffer (2:8, v/v, pH 7.4) solution and the corresponding photophysical data were summarized in Table 1. Compound **PI-Rh** had two major absorption bands centered at 323 nm (belonged to the **Rh** moiety), and at 374 nm (belonged to the **PI** moiety) (Fig. 1**A**, blank line). The UV–vis absorption spectral bands for the model reagent **Rh-1** (Fig. 1**A**, wine line) and **PI-1** confirmed this assignment (Fig. 1**A**, blue line).

Compound **PI-Rh** emitted yellow–green fluorescence. Its maximum emission band was at 540 nm (λ_{ex} = 370 nm) (Fig. 1**B**, black

Table 1
Photophysical characterizations of **PI**–derivatives, **Rh**–derivatives, and **PI-Rh.**

Compound	λ_{abs} (nm)[a]	λ_{em} (nm)[b]
PI-0	315	392
PI-1	374	450, 540
PI-2	361	445
Rh-0	555	586
Rh-1	321	436 (very weak)
Rh-2	555	586
PI-Rh	323, 374	540

[a] The major absorption band of dye.
[b] The major emission band of dye.

line), which was ascribed to the **PI** moiety. Compared its emission spectra with that for the model reagent **PI-1** (Fig. 1**B**, blue line), a similar emission band was observed. As anticipated, under the excitation of 370 nm, the characteristic emission band of the ring-opening of the Rhodamine could not be detected because of its closed–spirolactam moiety in compound **PI-Rh**.

Next, the photostability of compound **PI-Rh** in DMSO–PBS buffer (2:8, v/v, pH 7.4) solution was tested. Results showed that the initial fluorescence intensity of compound **PI-Rh** could be maintained above 98% when exposed to a Xe lamp (150 W) for 1 h (**Fig. S14**). These results indicated that compound **PI-Rh** had a good photostability and could be used in biological research.

*2.2.2. Sensing properties of compound **PI-Rh** for hydrazine*

2.2.2.1. Spectroscopic response toward hydrazine. First, the spectral response of **PI-Rh** toward hydrazine was investigated upon titration of **PI-Rh** with various concentration of hydrazine in DMSO–PBS buffer (2:8, v/v, pH 7.4) solution (Fig. 2**A**). Upon titration with hydrazine (0–20 equiv.), the two major absorption bands at 323 nm and 374 nm of **PI-Rh** gradually blue sifted to about 320 nm and 371 nm that belonged to the **PI** fluorophore, and no absorption band above 500 nm was observed. These results indicated that compound **PI-Rh** in the presence of excess hydrazine presented the **PI** fluorophore and the closed-spirolactam form of the **Rh** fluorophore.

Subsequently, we investigated the fluorescence spectra change of **PI-Rh** after addition of hydrazine under the same conditions. As shown in Fig. 2**B**, the free compound **PI-Rh** emitted yellow–green fluorescence with a maximum emission band at 540 nm. However, when hydrazine was gradually added to the solution of **PI-Rh**, the fluorescence intensity at around 540 nm decreased. Meanwhile, a new peak at 445 nm that belonged to the **PI** fluorophore appeared and increased. No opened–Rhodamine–based emission band was observed indicating that compound **PI-Rh** in the presence of hydrazine presented the closed–spirolactam form of the **Rh** fluorophore, which was consistent with the UV–vis absorption observation. An obvious isosbestic point at 511 nm indicated that the interaction between **PI-Rh** and hydrazine was the only reaction process (Scheme 1**)**. When adding 20 equiv. hydrazine, the fluorescence intensity at 445 nm reached saturation (Fig. 2**C**). At this time, an obvious emission color change could be easily observed. This obvious distinguishable fluorescence response enabled **PI-Rh** to visually and ratiometrically determine hydrazine. Fig. 2**D** showed that the fluorescence intensity ratio (I_{445}/I_{542}) was linear correlated with the concentrations of hydrazine over a concentration range of 0–120 μM (Y = 0.15637 + 431 06.61521 × X, R^2 = 0.9946). This result indicated compound **PI-Rh** was suitable for quantitative detection of hydrazine. The detection limit of **PI-Rh** was estimated to be 0.0632 μM (~2 ppb), which was lower than the concentration level (10 ppb) set by U.S. EPA [9].

To evaluate the response speed of **PI-Rh** for hydrazine, the I_{445}/I_{542} changes of **PI-Rh** in the presence or absence of hydrazine in DMSO–PBS buffer (2:8, v/v, pH 7.4) solution at room temperature was recorded and plotted against time (**Fig. S15**). The value of I_{445}/I_{542} enhanced significantly within 1 min, and a plateau was reached nearly in 30 min after addition of 200 μM hydrazine, demonstrating that **PI-Rh** was a fast responsive probe to hydrazine. Under identical conditions, the free **PI-Rh** exhibited almost no fluorescent changes. Next, the effect of pH on the fluorescence emission pattern of **PI-Rh** in the presence or absence of hydrazine in DMSO–PBS buffer (2:8, v/v, pH 7.4) solution at room temperature was evaluated using acid–base titration experiments. As shown in **Fig. S16**, **PI-Rh** was stable within pH range from 5.1 to 10.2. When **PI-Rh** was incubated with hydrazine, the fluorescence intensity at 445 nm hardly changed with the change of pH value, in the range of 5.1–10.2. These experimental results demonstrated that **PI-Rh** showed a good response to hydrazine in the pH range of 5.1–10.2, which could be used in environment and biology.

2.2.2.2. Proposed mechanism and confirmation of the product structures. We proposed the response mechanism of **PI-Rh** and hydrazine as depicted in Scheme 3. Firstly, the hydrogen bonds between the spirolactam of **PI-Rh** and hydrazine was formed, which could activate imine unit to improve its electrophilic ability and favor for the next chemoslective nucleophilic addition. Next, another hydrazine molecule attacked the activated C═N double bond to form the intermediate **II**, and followed by hydrolysis of the corresponding C—N linkage to generate intermediates **III** and **IV** respectively. **III** was the complex of **Rh-1** and hydrazine, and removal of one molecule of water from **IV** to produce compound **PI-2**. Thus, hydrazine played an important role in the fracture of C═N double bond in **PI-Rh**, which was both a reactant and a catalyst.

To clarify the above work mechanism of **PI-Rh** for hydrazine, relevant experimental data of HRMS, UV–vis absorption, fluorescence, and NMR spectra (^{1}H NMR and ^{13}C NMR) of the reaction mixture of **PI-Rh** with hydrazine were compared with those of **PI-Rh**, **Rh-1** and **PI-2**. As shown in **Fig. S17**, after mixing compound **PI-Rh** and excessive hydrazine for 30 min at ambient temperature, two peaks at *m*/*z* value of 337.1445 and 485.2916 corresponding to the products [**PI-2**+H]$^+$ and [**Rh-1**+H]$^+$ were observed, and there was no peak of [**PI-Rh**+2DMF+H_2O+K^+]$^+$ (*m*/*z* 991.4633). This result indicated that **PI-Rh** was completely converted to **PI-2** and **Rh-1** by reaction with excess hydrazine. Compared the UV–vis absorption and fluorescence spectra with those for the model regents **PI-2** and **Rh-1** (**Fig. S18**), we could find that the reaction products of **PI-Rh** with excess hydrazine in DMSO–PBS buffer (2:8, v/v, pH 7.4) solution at ambient temperature were **PI-2** and **Rh-1**.

Next, the work mechanism was further supported by ^{1}H NMR and ^{13}C NMR spectra titration analysis in detail (Fig. 3). As illustrated in Fig. 3**A**, the proton signal (H_a) at 8.08 ppm of **PI-Rh** corresponded to the —C**H**═N— group. After mixing compound **PI-Rh** and excess hydrazine for 30 min, the proton signal of H_a disappeared completely and a new signal at 7.78 corresponding to the —C**H**═N—NH_2 group (H_b) of **PI-2** appeared. Moreover, the other aromatic and alkyl proton signals created from the reaction of **PI-Rh** and hydrazine were also corresponding to those of **PI-2** and **Rh-1**. For the ^{13}CNMR spectra, in Fig. 3**B**, after reaction with hydrazine, the carbon signals at 161.84 ppm (C_a) corresponded to the —**C**H═N— group and at 58.82 ppm (C_1) adjacent to —**C**H═N— group of **PI-Rh** disappeared completely. Meanwhile, a new carbon signal at 161.00 ppm corresponding to the carbon signal of C_b of **PI-2** appeared. Furthermore, the characteristic signals at 167.54 ppm (Cc) and 64.62 ppm (C_2) for the closed–spirolactam form of the **Rh** fluorophore did not disappear, which indicated that the closed–spirolactam moiety in RDM was not opened before and after reaction. Additionally, the other carbon signals in the product were corresponding to those of **PI-2** and **Rh-1**. These above NMR data

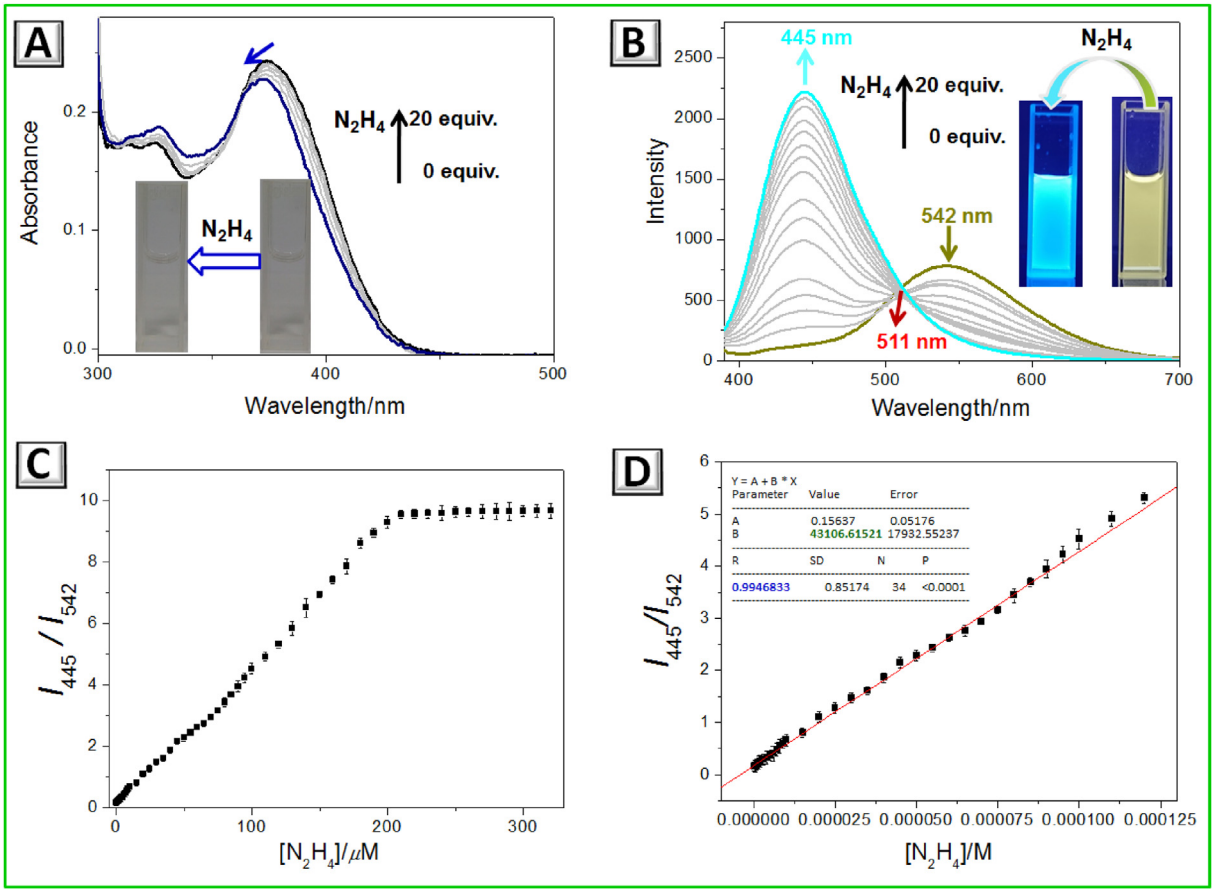

Fig. 2. Absorption (**A**) and emission spectra (**B**) changes s of **PI-Rh** (10 μM) with adding different equivalent of hydrazine (0–20 equiv.) in DMSO–PBS buffer (2:8, v/v, pH 7.4) solution at ambient temperature. (**C**) The fluorescence intensity ratio (I_{445}/I_{542}) versus concentration of hydrazine. (**D**) Plot the fluorescence intensity ratios (I_{445}/I_{542}) against concentration of hydrazine. Excitation wavelength is 370 nm.

effectively validated our proposed work mechanism of probe **PI-Rh** to hydrazine (Schemes 1 and 4).

*2.2.3. Sensing properties of compound **PI-Rh** for Hg^{2+}*

2.2.3.1. Spectroscopic response toward Hg^{2+}. Next, we investigated the capability of **PI-Rh** for sensing Hg^{2+} in DMSO–PBS buffer (2:8, v/v, pH 7.4) solution (Fig. 4). When an increasing amount of Hg^{2+} was added to the solution of **PI-Rh**, the fluorescence intensity at around 540 nm decreased, while, a broad emission band at about 420 nm belonged to the **PI** fluorophore gradually increased (Fig. 4**A**). Meanwhile, a new emission band at about 585 nm belonged to the opened–**Rh** fluorophore became more and more obvious. These results indicated that compound **PI-Rh** in the presence of excess Hg^{2+} presented the **PI** fluorophore and the opened–spirolactam form of the **Rh** fluorophore. Additionally, we were surprised to find that the color of the solution emitted near white fluorescence. The CIE chromaticity coordinates of the reaction mixture of **PI-Rh** with Hg^{2+} was (0.382, 0.348), which was very close to that of pure white light (0.330 ± 0.050, 0.330 ± 0.050) (Fig. 4**B**). As far as we know, this was the first reported probe to sense Hg^{2+} aqueous solution with a white fluorescence.

For the UV–vis absorption spectra, when Hg^{2+} was gradually added to the solution of **PI-Rh**, the major band at about 373 nm of **PI-Rh** gradually decreased. Meanwhile, a new band centered at 563 nm that belonged to the opened–spirolactam form of the **Rh** fluorophore appeared and increased (Fig. 5**A**). In addition, there was an obvious isosbestic point at 490 nm. When 30 equiv. Hg^{2+} was added, the absorbance at 563 nm reached saturation, and the color of **PI-Rh** solution turned from colorless to pink. The absorption intensity ratio (A_{563}/A_{373}) was linear correlated with the concentration of Hg^{2+} over a wide range of 0–100 μM (Y = 0.01004 + 32304.0913 × X, R^2 = 0.9989). This result indicated that **PI-Rh** was suitable for quantitative detection of Hg^{2+} (Fig. 5**B**). The detection limit of **PI-Rh** for Hg^{2+} was estimated to be 0.0101 μM (~2 ppb), which was within the concentration level (~2 ppb) set by of U.S. EPA.

Next, we examine the response time of **PI-Rh** with Hg^{2+} in DMSO–PBS buffer (2:8, v/v, pH 7.4) solution at room temperature. The absorption band at 563 nm promptly increased, and a plateau was reached within minutes after the addition of Hg^{2+}, indicating this response was very fast (**Fig. S19**). Besides, we investigated the applicable pH range of **PI-Rh** by UV–vis absorption spectra. On the one hand, under a strong acidic condition (pH < 4), the free **PI-Rh** molecule undergone H^+–catalyzed ring-opening to generate a characteristic absorption band at 563 nm. However, at the same pH, the absorbance intensity at 563 nm of **PI-Rh** in the presence of Hg^{2+} was stronger than those in the absence of Hg^{2+}. This result clear indicated that the spectra changes of **PI-Rh** with Hg^{2+} were mainly due to Hg^{2+} ion (**Fig. S20**). On the other hand, at a pH range from 4.2 to 10.2, **PI-Rh** was stable and it could be employed to detect Hg^{2+}. These experimental results demonstrated that **PI-Rh** showed a good UV–vis absorption response toward Hg^{2+} in the pH range of 4.2–10.2, which could be used in environment and biology.

2.2.3.2. Proposed mechanism and confirmation of the product structures. We proposed the response mechanism of **PI-Rh** and Hg^{2+} as depicted in Scheme 4. Firstly, the binding of the Hg^{2+} ion with **PI-**

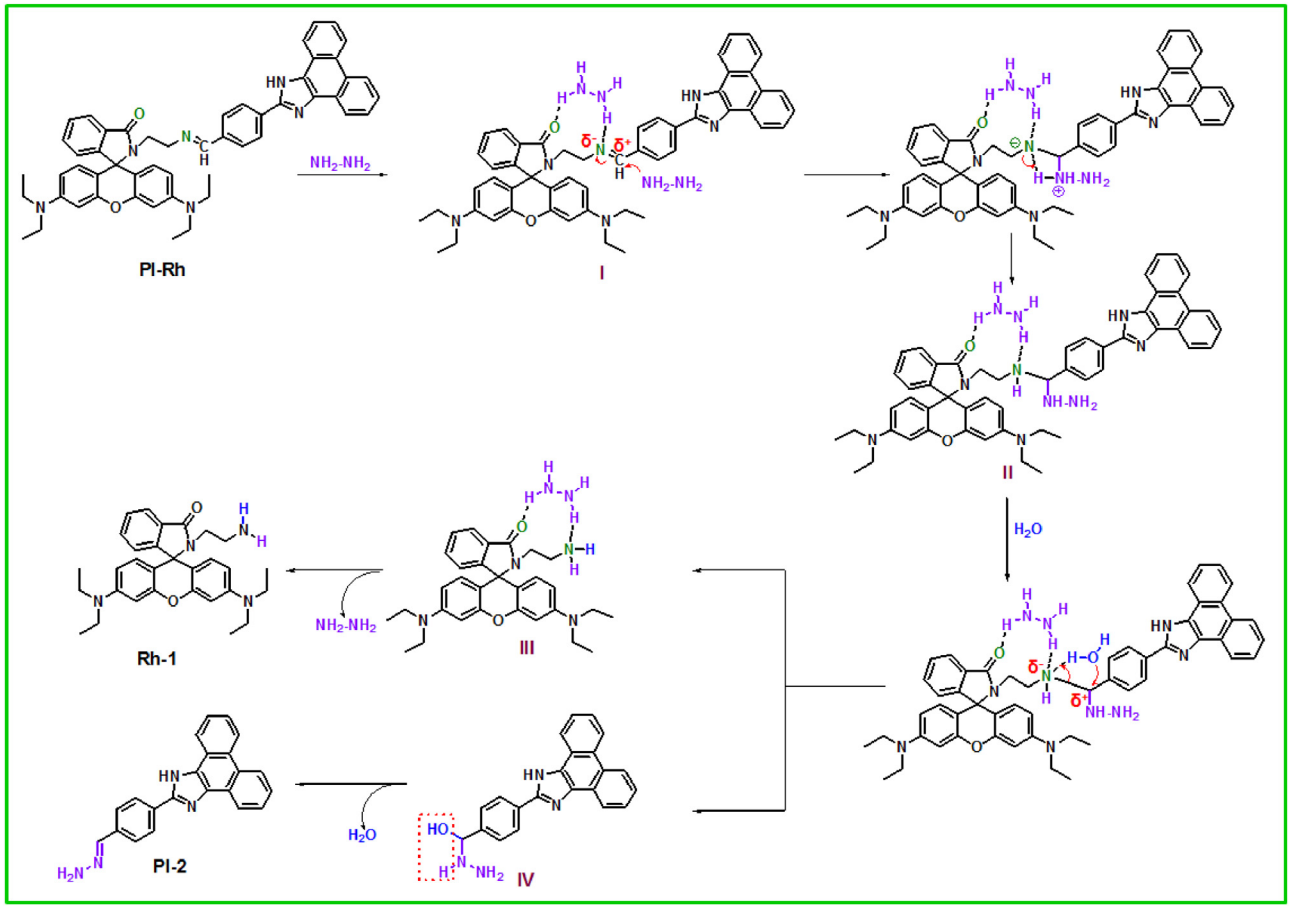

Scheme 3. Probable sensing mechanism of hydrazine by **PI-Rh**.

Rh inducing the ring opening of the spirolactam of **PI-Rh** generated the complex **I**, which could activate imine unit to improve its electrophilic ability. Next, a water molecule attacked the activated C=N double bond to form intermediate **III** and compound **PI-1**, respectively. **III** lost one molecule $HgCl_2$ to form **Rh-2**. Thus, $HgCl_2$ played a catalyst role in the chemodosimetric hydrolysis of **PI-Rh**.

To further clarify the above work mechanism of **PI-Rh** for Hg^{2+}, relevant experimental data of HRMS, UV–vis absorption, fluorescence, and NMR spectra (^1H NMR and ^{13}C NMR) of the reaction mixture of **PI-Rh** with Hg^{2+} were compared with those of **PI-Rh**, **Rh-1** and **PI-2**. As shown in **Fig. S21**, after adding 30 equiv. Hg^{2+} to the solution of **PI-Rh** for about 0.8 min, we could see a mass spectral peak at *m*/*z* 1061.2995 belonging to [**PI-Rh**+$HgCl_2$]$^+$. When the reaction time was about 1.7 min, we could see two mass spectral peaks at *m*/*z* 323.1181 and *m*/*z* 485.2919 belonging to the products [**PI-1**+H]$^+$ and [**Rh-2**+H]$^+$. The peak of [**PI-Rh**+$HgCl_2$] $^+$ (*m*/*z* 1061.2995) was not find, which demonstrated that **PI-Rh** was completely converted to **PI-1** and **Rh-2** by reaction with excess hydrazine within minutes. This result was compatible with the UV–vis absorption observation (**Fig. S19**). Compared the UV–vis absorption and fluorescence spectra with those for the model regents **PI-1** and **Rh-2** (**Fig. S22**), we could find that the reaction products of **PI-Rh** with $HgCl_2$ in DMSO–PBS buffer (2:8, v/v, pH 7.4) solution at ambient temperature were **PI-1** and **Rh-2**.

Next, the work mechanism was further supported by ^1H NMR and ^{13}C NMR spectra titration analysis in detail (Fig. 6). As illustrated in Fig. 6**A**, after reaction with excess $HgCl_2$, the proton signal of H_a disappeared completely and a new proton signal at 10.11 ppm corresponding to the aldehyde proton H_b of **PI-1** appeared. Moreover, the other aromatic and alkyl proton signals created from the hydrolysis reaction were also corresponding to those of **PI-1** and **Rh-1**+$HgCl_2$. For the ^{13}C NMR spectra, in Fig. 6**B**, after hydrolysis reaction, carbon signals C_a and C_1 disappeared completely. Meanwhile, a new carbon signal at 192.80 ppm corresponding to the carbon signal of C_b of **PI-1** appeared. Furthermore, the characteristic signals at 167.54 ppm (Cc) and 64.62 ppm (C_2) for the spirolactam form of the **Rh** fluorophore also disappeared completely, which indicated that the spirolactam moiety in RDM was opened after the Hg^{2+}–induced hydrolysis of **PI-Rh**. Additionally, the other carbon signals in the product were corresponding to those of **PI-1** and **Rh-1**+$HgCl_2$. These above NMR data effectively validated our proposed work mechanism that the binding of the $HgCl_2$ with **PI-Rh** induced the ring-opening of the spirolactam of **PI-Rh**, and promoted the hydrolysis of the imine linkage to generate the corresponding mixture of aldehye **PI-1** and Rhodamine B derivative **Rh-2** (**Schemes 2 and 5**).

2.3. DFT calculation

Next we used density functional theory (DFT) and TDDFT methods for study of the spectral transduction of **PI-Rh** for identifying hydrazine and Hg^{2+}, respectively. We found that the different spectral changes of **PI-Rh** in response to hydrazine and Hg^{2+}, could be predicted by the TDDFT theoretical calculations of the Gaussian 03 program, based on the ground–state geometries of the compounds, respectively [97].

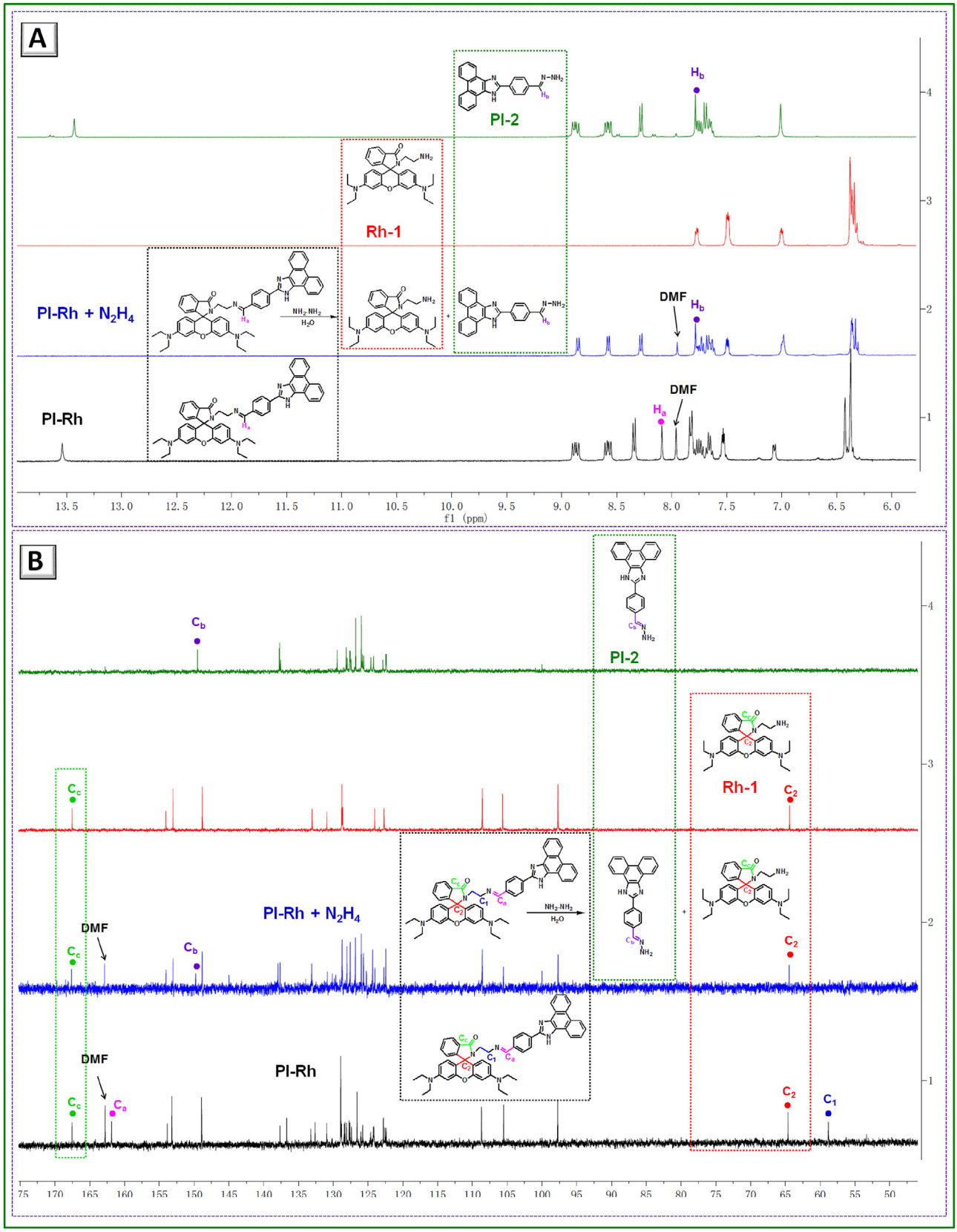

Fig. 3. ^{1}H NMR (**A**) and ^{13}C NMR (**B**) spectra of **PI-Rh** (3.5 mM), **PI-2** (3.5 mM), **Rh-1** (3.5 mM), and **PI-Rh** (3.5 mM) after reaction with hydrazine (20 equiv.) in DMSO–d_6, respectively.

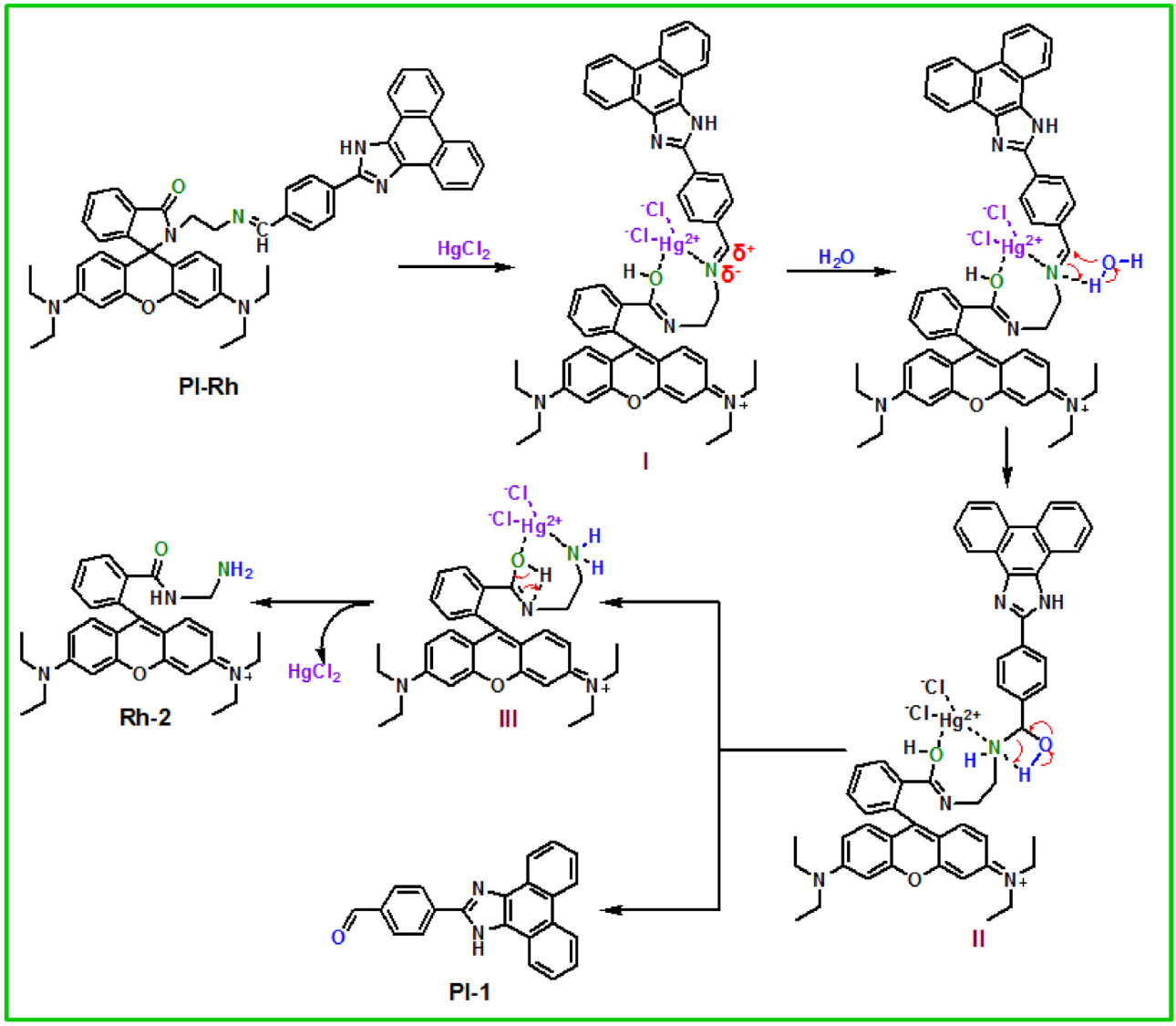

Scheme 4. Probable sensing mechanism of Hg^{2+} by **PI-Rh**.

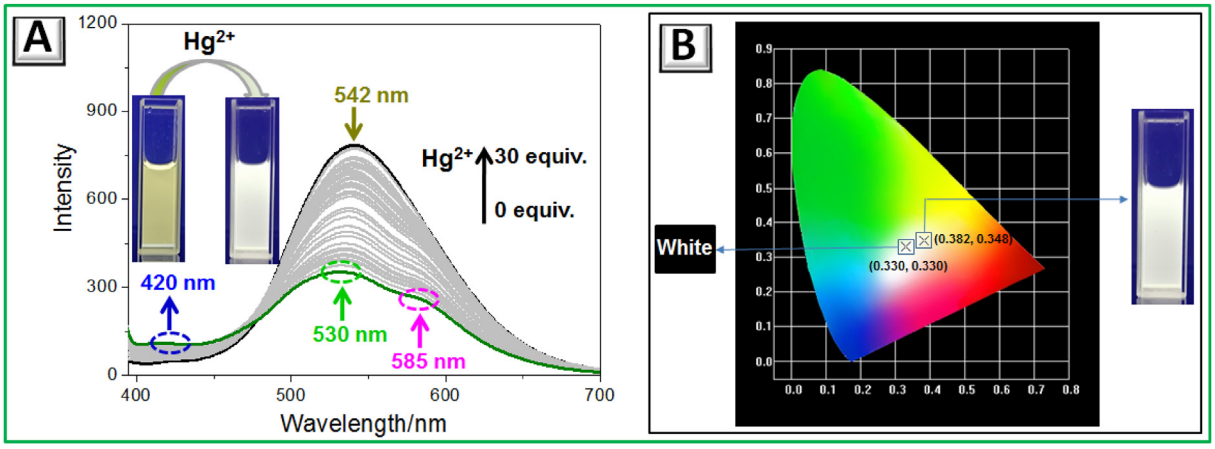

Fig. 4. (**A**) Emission spectra changes of **PI-Rh** (10 μM) with adding different equivalent of Hg^{2+} (0–30 equiv.) in DMSO–PBS buffer (2:8, v/v, pH 7.4) solution at ambient temperature. (**B**) The CIE chromaticity coordinates of the reaction mixture of **PI-Rh** with Hg^{2+}. Excitation wavelength is 370 nm.

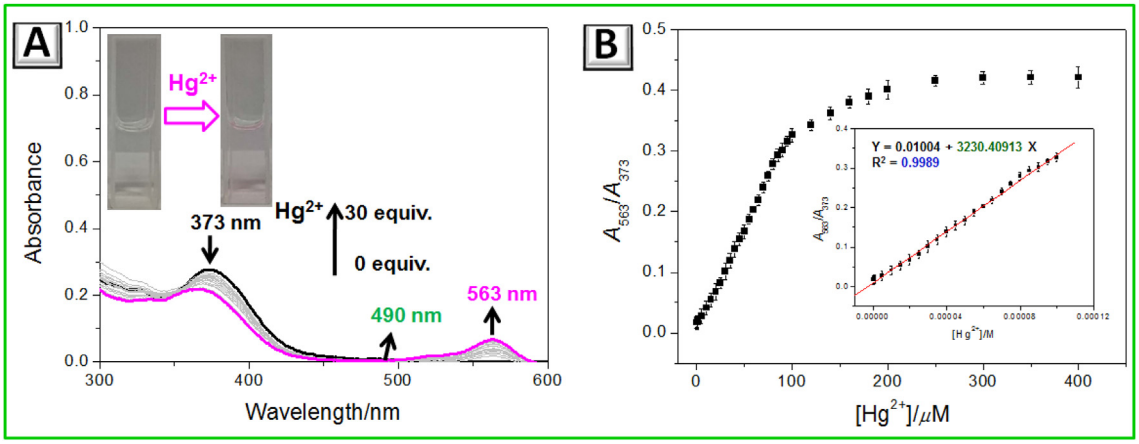

Fig. 5. (**A**) Absorption spectra changes of **PI-Rh** (10 μM) with adding different equivalent of Hg^{2+} (0–30 equiv.) in DMSO–PBS buffer (2:8, v/v, pH 7.4) solution at ambient temperature. (**B**) The absorption intensity ratio (A_{563}/A_{373}) versus concentration of Hg^{2+}. Inset: plot of the absorption intensity ratio (A_{563}/A_{373}) against concentration of Hg^{2+}.

First, the geometry optimization of **PI-Rh**, **PI**, and **Rh-1** were optimized with DFT method, respectively. Then, the UV–vis absorption of **PI-Rh**, **PI**, and **Rh-1** were calculated with the TDDFT method on the basis of the optimized S_0 state geometry, respectively. As shown in Fig. 7, for compound **PI-Rh**, the highest occupied orbital (HOMO) was distributed in the xanthenecore moiety, while the lowest unoccupied orbital (LUMO) was distributed in the **PI** moiety; while for **PI-2**, the isosurface was mainly localized within the donor part (**PI** core) in the HOMO and moved to the acceptor part (—$CHNNH_2$) in the LUMO; in the case of **Rh-1**, the HOMO was completely distributed in the xanthenecore moiety, and the LUMO was completely distributed in the closed–spirolactam part. The gaps between HOMO and LUMO level of **PI-Rh**, **PI**, and **Rh-1** were 3.4526 eV (396 nm), 3.6733 eV (363 nm), and 4.3344 eV (326 nm), respectively, indicating the blue–shift of maximum absorption of **PI-Rh** when reacted with hydrazine hydrate.

The same calculation method was applied for **PI-Rh** detecting of Hg^{2+}. As shown in Fig. 8, for **PI-1**, the isosurface was mainly localized within the **PI** core (donor part) in the HOMO and moved to the benzaldehyde group (acceptor part) in the LUMO, which was similar to that of **PI-2**. In the case of **Rh-2**, the HOMO was completely distributed in the ethylenediamine moiety, while the LUMO was almost distributed in the xanthenecore, which was opposite to that of **Rh-2**. This wide divergence in the distribution of the isosurface indicated that the spectral properties of compounds **Rh-2** and **Rh-1** were quite different. The gaps between HOMO and LUMO level of **PI-1**, and **Rh-2** were 3.3934 eV (397 nm), and 2.6533 eV (554 nm), respectively, indicating the red–shift of maximum absorption of **PI-Rh** when reacted with $HgCl_2$ aqueous solution.

The above theoretically predicted maximum absorption bands at 396 nm, 363 nm, 326 nm, 397 nm, and 554 nm for **PI-Rh**, **PI-2**, **Rh-1**, **PI-1**, and **Rh-2**, were quite well with the experimental observation at 374 nm, 361 nm, 321 nm, 374 nm, and 555 nm, respectively (Table 1, Figs. 1, 2, and 5). And these theoretical calculation results further verified the experimental results.

2.4. Selectivity and interference capability

In order to investigate the sensing specificity of **PI-Rh** for Hg^{2+} ion and hydrazine, the selectivity experiments were carried out by using UV–vis absorption and fluorescence spectra. Metal ions (Ag^+, Zn^{2+}, Pd^{2+}, Al^{3+}, Ca^{2+}, Cu^{2+}, Cd^{2+}, Mg^{2+}, Co^{2+}, Fe^{3+}, Cr^{3+}, Li^+, Mn^{2+}, and Ni^{2+}) and nucleophilic reagents (NH_2–OH, NH_3, Et_2NH, Et_3N, $^nPrNH_2$, CN–, HS–, HSO_3–, Hcy, GSH, and Cys) were investigated. As shown in Fig. 9**A**, (i) only Hg^{2+} ion triggered an obvious red shift of **PI-Rh**; (ii) Adding hydrazine or NH_2–OH could induce a visible change in absorbance of **PI-Rh**; (iii) Addition other analytes, the UV–vis absorption of **PI-Rh** remained almost unchanged. These results indicated that **PI-Rh** was high selective toward Hg^{2+} ion over other competitive analytes. For the fluorescence spectra (Fig. 9**B**), (i) hydrazine and NH_2–OH induced an obvious blue shift, and hydrazine induced stronger (*ca.* 2.3 times compared to that with NH_2–OH) the fluorescent intensity of **PI-Rh**; (ii) Addition Hg^{2+} could induce a decrease in fluorescent intensity of **PI-Rh**; (iii) Fe^{3+} and Pd^{2+} led to an almost complete fluorescence quenching; (iv) the fluorescence spectrum of **PI-Rh** remained almost unchanged by addition of the other analytes. Thus, **PI-Rh** was high selective toward hydrazine and Hg^{2+} ion over other competitive analytes. Also, hydrazine and Hg^{2+} ion induced obvious fluorescence emission changes from yellow-green to cyan and white, respectively, enabled naked eye detection of hydrazine and Hg^{2+} ion.

To validate the non–interference of other metal ions and nucleophilic reagents, competition experiments of **PI-Rh** were carried out in the presence of excess concentrations of other commonly coexisting materials in DMSO–PBS buffer (2:8, v/v, pH 7.4) solution (**Figs. S22 and S23**). These results indicated that **PI-Rh** could effectively detect N_2H_4 and Hg^{2+} even if there were excess other competitive metal ions and nucleophilic reagents in the solution.

After establishing the non-interference of metal ions and nucleophilic reagents, it was imperative to estimate the effect of N_2H_4 in the detection of Hg^{2+}, and vice versa. Addition N_2H_4 (30 equiv.) to the solution of **PI-Rh** (10 μM), a small blue–shift of the maximum absorption band and an obvious blue–shift of fluorescence emission were obtained (**Fig. S24**). When 30 equiv. of Hg^{2+} was added to the solution of **PI-Rh**, the fluorescence intensity at around 540 nm decreased, while, two broad emission bands at about 420 nm and 585 nm gradually increased. Under comparable conditions, on the one hand, addition of only 30 equiv. of Hg^{2+} to the solution that obtained from **PI-Rh** (10 μM) and 30 equiv. of N_2H_4 developed an absorption band at about 563 nm (**Fig. S24A**) and enhanced the emission intensity at about 585 nm (**Fig. S24B**). These results could be attributed to the Hg^{2+}–selective inducing the opening of **Rh** spirolactam form. On the other hand, upon addition of N_2H_4 (30 equiv.) to the solution that obtained from **PI-Rh** (10 μM) and 30 equiv. of Hg^{2+}, a new emission band centered at about 445 nm appeared (**Fig. S24B**). This result could be attributed to the N_2H_4–selective inducing the condensation with **PI-1**. Thus, the absorption and fluorescence profiles displayed by **PI-Rh** to the addition of N_2H_4 and Hg^{2+} appear to permit the selective detection of N_2H_4 and Hg^{2+} in isolation and in combination.

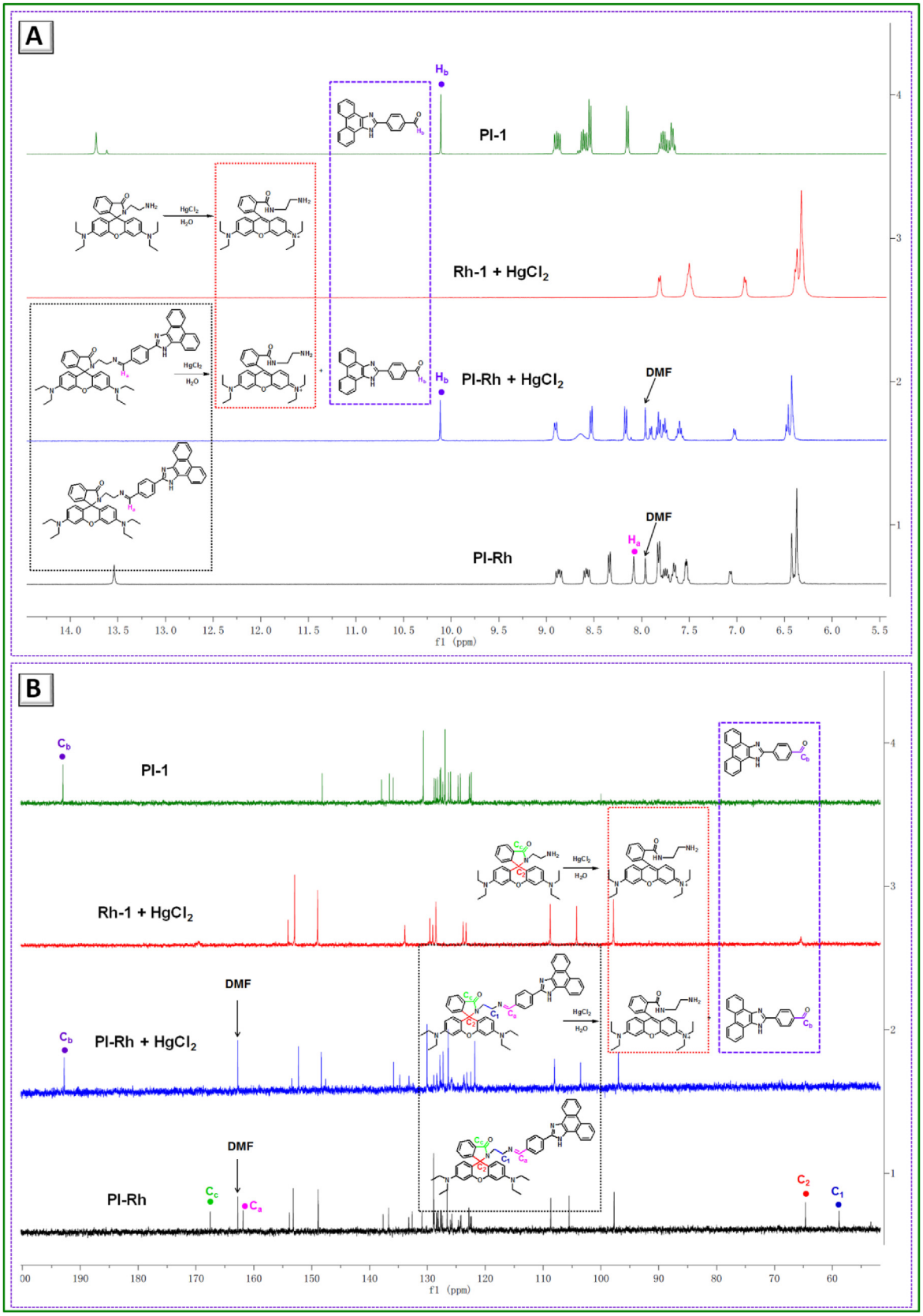

Fig. 6. ^{1}H NMR (**A**) and ^{13}C NMR (**B**) spectra of **PI-Rh** (3.5 mM), **PI-1** (3.5 mM), **Rh-1** (3.5 mM) + $HgCl_2$ (30 equiv), and **PI-Rh** (3.5 mM) + $HgCl_2$ (30 equiv.) in DMSO d_6: D_2O = 8:1, respectively.

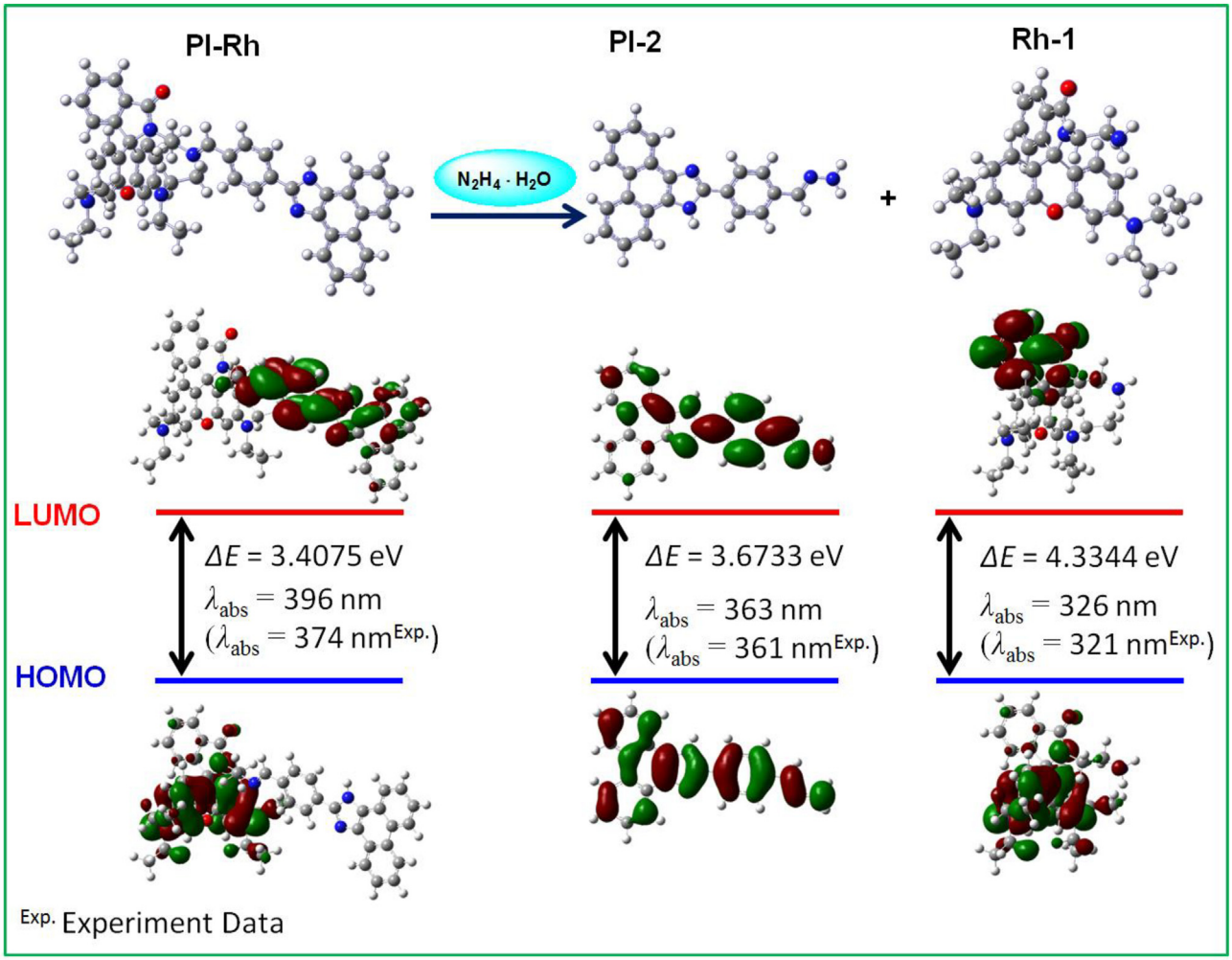

Fig. 7. Optimized geometries, the potential energy differences (ΔE) of HOMO–LUMO orbitals, and their corresponding predicted major absorption bands (λ_{abs}) of **PI-Rh**, **PI-2**, and **Rh-1** calculated on the DFT level using a B3LYP/6-311G, respectively.

2.5. Application

2.5.1. Application for detection N_2H_4

*2.5.1.1. Performance of **PI-Rh** in sensing N_2H_4 in real water sample.* Because hydrazine has been widely used in medicine, agriculture and chemical industry, detection of trace amounts of hydrazine in actual water is very necessary. Initially, the linear plotting of the fluorescence intensity ratios (I_{445}/I_{542}) of **PI-Rh** (10 μM) versus concentration of hydrazine (0–500 nM) in redistilled water was made (**Fig. S26**). Next, the actual water samples (local lake water and tap water) were centrifuged and filtered, and followed by incubation with **PI-Rh** (10 μM). No obvious fluorescence changes were observed. Then, the adding an aliquot of hydrazine to the real water samples determined by **PI-Rh** was detailed in **Table S1**. The recovery rates of hydrazine based on the linear plotting were found to be 98.1–101.4% for all the spiked samples, indicating that **PI-Rh** could reliably and effectively detect hydrazine quantitatively in realistic water samples.

2.5.1.2. Detection of N_2H_4 in soil. To explore the environmental analysis, we try to apply **PI-Rh** for detection of hydrazine hydrate in various soils (field soil, sand soil and clay soil). Firstly, 3 mL of the aqueous solution of hydrazine (0.5 mM, 2.0 mM) was sprayed evenly on various soils (~1g), respectively. Obviously, it was difficult to find out whether hydrazine hydrate existed in soil with naked-eye (Fig. 10). Next, we poured the soil in the absence and presence of hydrazine hydrate into a glass bottle with an aqueous solution of **PI-Rh** (0.1 mM), respectively. After a few minutes, we were surprised to find out that the fluorescence changes of the solution containing hydrazine–treated soil were quite obviously and the response speed was very quickly in all soils (Fig. 10 and **Fig. S27**). However, there were no fluorescence changes for the hydrazine–unpretreated soils, even for 1 day. These results showed that **PI-Rh** could be used to detect hydrazine hydrate for environmental analysis.

2.5.1.3. Portable test paper strip for the detection of gaseous N_2H_4. The above results demonstrated that **PI-Rh** showed high selectivity and responsiveness with a visualization of N_2H_4 fluorescence detection. Hence, we tried to develop the feasibility of the portable **PI-Rh**–based test paper for N_2H_4 detection. Soak an appropriate size cellulose filter paper strips into a solution of **PI-Rh** (1 mM in DMSO) for 30 min at ambient temperature, and dried. As shown in Fig. 11**A and 11C**, **PI-Rh**–impregnated test paper emitted an emission at ~525 nm with bright yellow–green fluorescence. When **PI-Rh**–impregnated test paper was hung in respective cuvettes containing an increase concentrations of N_2H_4 solution (0–1 mM) at ambient temperature for 30 min, the UV color of the test paper gradually changed from yellow–green to dark cyan and finally to blue with an emission at ~400 nm (Fig. 11**C**). In addition, the response was

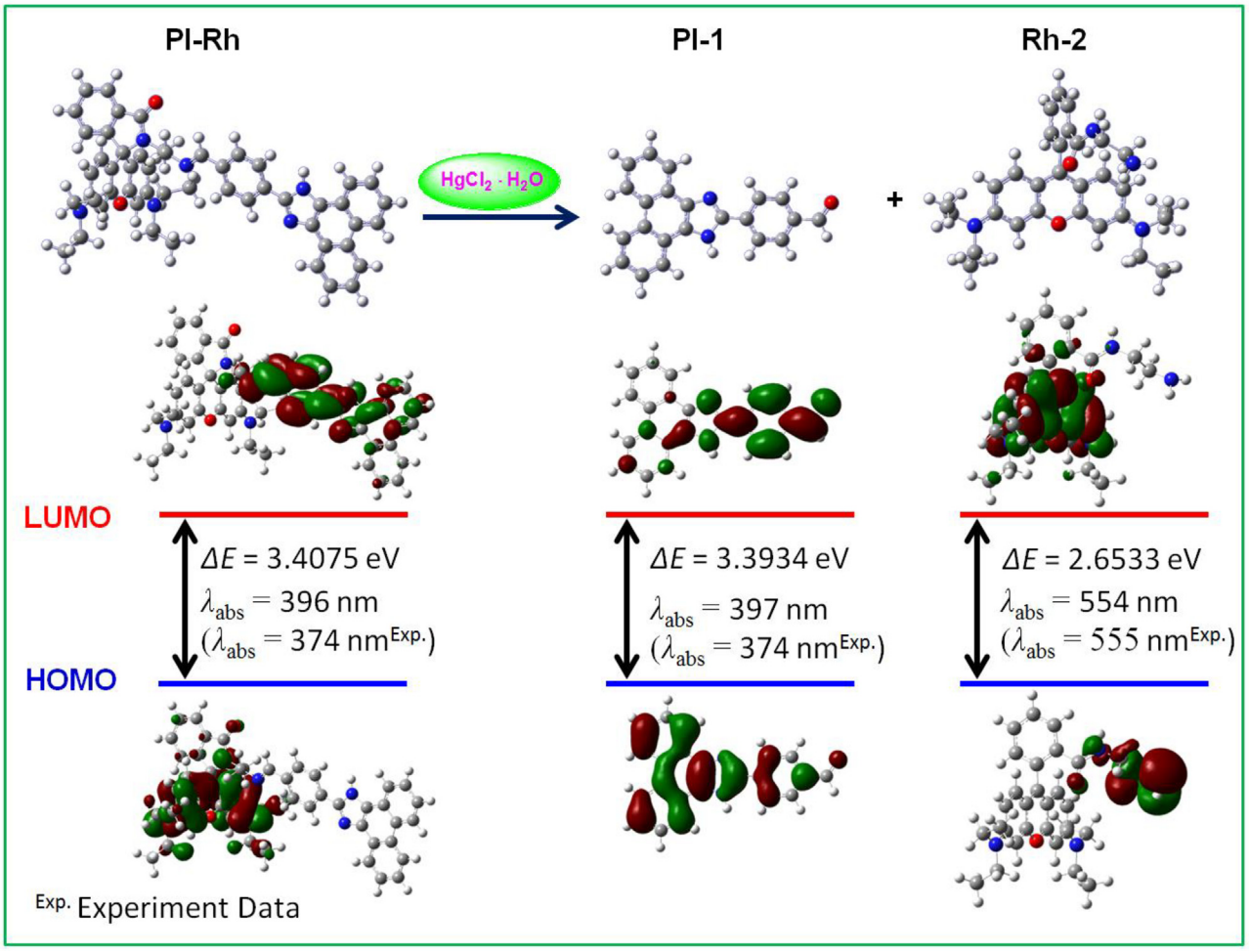

Fig. 8. Optimized geometries, the potential energy differences (ΔE) of HOMO–LUMO orbitals, and their corresponding predicted major absorption bands (λ_{abs}) of **PI-Rh**, **PI-1**, and **Rh-2** calculated on the TDDFT level using a B3LYP/6–311G, respectively.

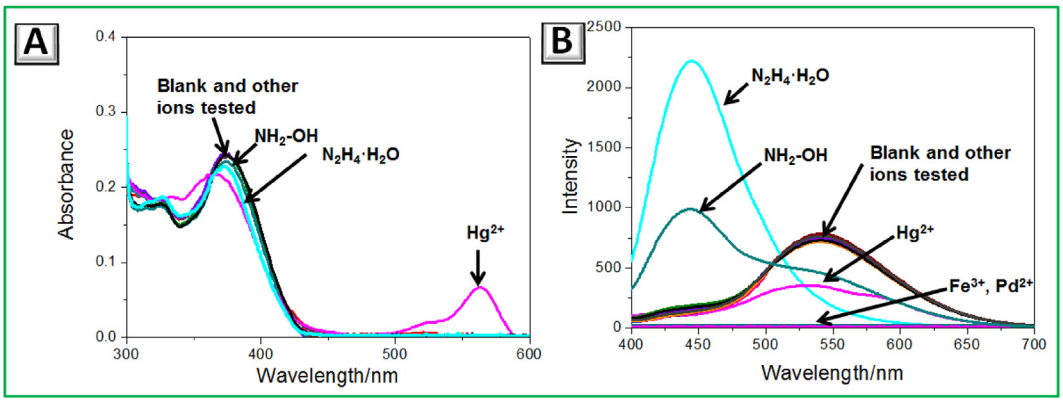

Fig. 9. Absorption (**A**) and emission (**B**) spectra changes of **PI-Rh** (10 μM) with adding 30 equiv. of metal ion or nucleophilic reagent in DMSO–PBS buffer (2:8, v/v, pH 7.4) solution at room temperature. Excitation wavelength is 370 nm.

very fast and it was easy to distinguish the UV color change. Results shown in Fig. 11**B** indicated that the **PI-Rh**–impregnated test paper and its stimulus response paper had an excellent fluorescent stability in an ambient atmosphere and temperature. The above satisfactory results enabled **PI-Rh** to visually and ratiometrically determine N_2H_4 in **PI-Rh**–impregnated test paper. The results were shown in Fig. 11**D**, the fluorescence intensity ratio (I_{445}/I_{542}) was linear correlated with the concentrations of hydrazine (0.001–0.5 mM) (Y = 0.01779 + 9244.72801 × X, R^2 = 0.99369), indicating the suitability of **PI-Rh**-impregnated test paper for semiquantitative detection of N_2H_4. The calculated detection limit was estimated to be 0.2793 μM (8.93 ppb).

2.5.2. Application for detection Hg^{2+}

*2.5.2.1. Performance of **PI-Rh** in sensing Hg^{2+} in real water sample.* The previous experimental results revealed that compound **PI-**

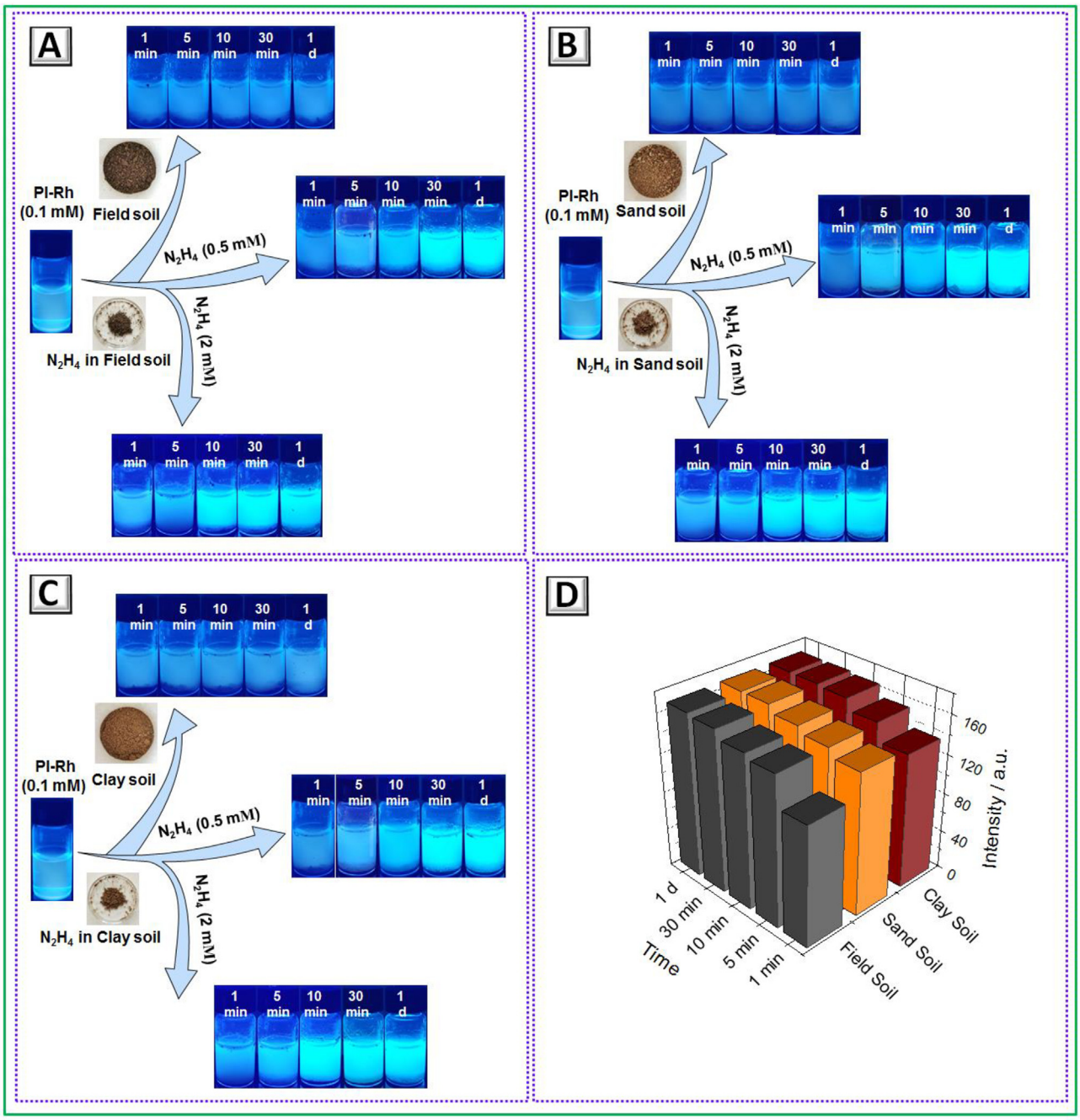

Fig. 10. Photographs of 3 mL **PI-Rh** solution in deionized water (0.1 mM, 2% DMSO, v/v) after upon addition of various soils. (**A**) Photographs for field soil. Top: N_2H_4–untreated, Middle: moistened with N_2H_4 (0.5 mM), Bottom: moistened with N_2H_4 (2.0 mM). (**B**) Photographs for sand soil. Top: N_2H_4–untreated, Middle: moistened with N_2H_4 (0.5 mM), Bottom: moistened with N_2H_4 (2.0 mM). (**C**) Photographs for clay soil. Top: N_2H_4–untreated, Middle: moistened with N_2H_4 (0.5 mM), Bottom: moistened with N_2H_4 (2.0 mM). (**D**) Relative fluorescence intensity of solutions as shown in panels (**A**, **B**, and **C**) for the soil moistened with N_2H_4 (0.5 mM).

Rh could ratiometrically detect Hg^{2+} in a wide concentration range using UV–vis absorption well. Thus, the absorption mode was preferred for examining the practicability of **PI-Rh** to detect Hg^{2+} in real water samples. Initially, the linear plotting of the ratio of the absorption intensity ratio (A_{563}/A_{373}) versus concentration of Hg^{2+} (0–200 nM) in redistilled water was made (Fig. S28). Then, the adding amount of Hg^{2+} in tap water and lake water determined by **PI-Rh** was detailed in **Table S2**. The recovery rates of Hg^{2+} based on the linear plotting were found to be 96.1–99.3% and 101.2–107.4% in tap water and lake water samples, respectively, indicating that **PI-Rh** could reliably and effectively detect Hg^{2+} in actual water samples.

2.5.2.2. Portable test paper strip for the detection of Hg^{2+}. The successful detection of N_2H_4 encouraged us to study whether the **PI-Rh**–impregnated test paper could be used to detect Hg^{2+}. Soak the prepared **PI-Rh**–impregnated test papers into different concentrations of Hg^{2+} solutions for 1 h, and dried. Naked–eye color changes could be distinguished in a range of 0–200 μM of Hg^{2+}. The visual recognition ability for Hg^{2+} was *ca.* 5 μM under ambient

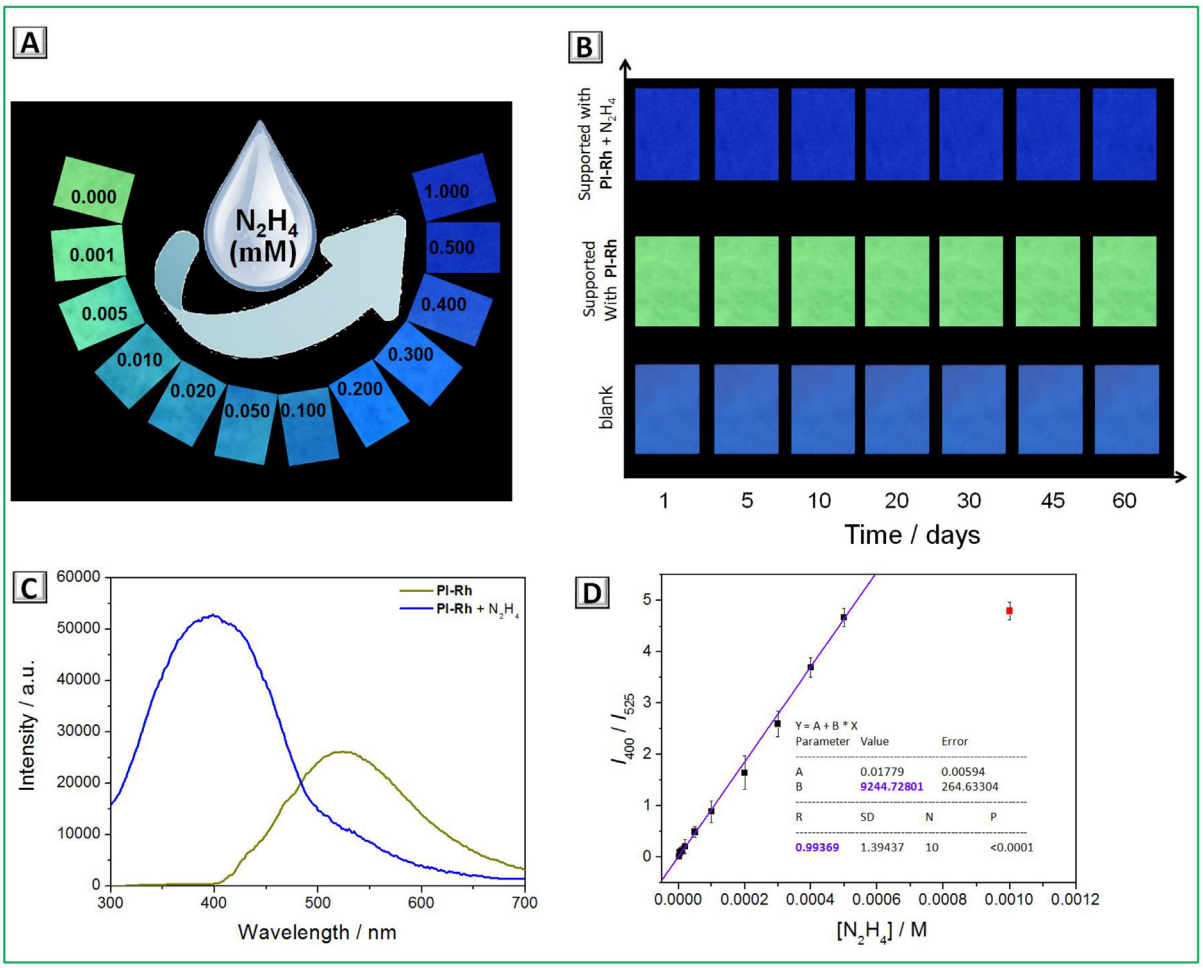

Fig. 11. (**A**) Visualization detection of N_2H_4 using the test paper supported with **PI-Rh**. These photos were taken under 365 nm UV light. (**B**) The stability of fluorescent paper strips within 60 days, from bottom to top are blank (filter paper), test paper supported with **PI-Rh** (1 mM), and test paper supported with **PI-Rh** (1 mM) + N_2H_4 (0.5 mM), respectively. (**C**) Fluorescence spectra of the **PI-Rh**–impregnated test paper and followed treated by N_2H_4. (**D**) Plot of test paper color change (I_{400}/I_{525}) versus concentration of N_2H_4.

light, and *ca.* 0.5 μM under a hand–hold UV lamp, respectively (Fig. S29). Compared with N_2H_4, the detection effect of the **PI-Rh**–impregnated test paper for Hg^{2+} was a little bit worse.

3. Conclusions

In conclusion, a new multifunctional phenanthroimidazole–Rhodamine conjugate probe **PI-Rh** has been develpoed for the detection of both hydrazine and mercury ion, induvidually and collectively, with different fluorescence outputs. The sensing mechanisms of **PI-Rh** for hydrazine and mercury ion were investigated in detail by HRMS, UV–vis absorption spectroscopy, fluorescence spectroscopy, NMR (^1H and ^{13}C) titration and control experiments, respectively. Probe **PI-Rh** showed good sensitivity and fast response for hydrazine and mercury ion at ppb levels, and precluded interference by other competitive ions and demonstrated high selectivity in solutions with obvious fluorescence color changes. In addition, the UV–vis absorption changes of **PI-Rh** for hydrazine and mercury ion were rationalized by DFT and TDDFT calculations. All the analysis and application results showed that not only the aqueous solution of **PI-Rh** could used as an effective probe for hydrazine detetion in actual water samples and in soil, but also **PI-Rh** was successfully fabricated into paper–based test stripes for visual, rapid, and real–time detection of gaseous hydrazine with a low detection limit. Besides, compound **PI-Rh** could be applied to effectively detect mercury ion in both colorimetric and ratiometric mode. Moreover, it could be successfully used for analyzing mercury ion in real water, and the facile **PI-Rh**–impregnated test paper was also well exploited for naked–eye detection of Hg^{2+}.

CRediT authorship contribution statement

Xiaofeng Yang: Conceptualization, Methodology, Writing - original draft, Funding acquisition. **Yiming Ding:** Investigation, Data curation. **Yexin Li:** Software, Funding acquisition. **Mei Yan:** Validation, Funding acquisition. **Yu Cui:** Validation. **Guoxin Sun:** Writing - review & editing.

Declaration of Competing Interest

The authors declare that they have no known competing financial interests or personal relationships that could have appeared to influence the work reported in this paper.

Acknowledgements

This work was supported by the National Natural Science Foundation of China (Grants 21708013, 21675064, 51473067), the Natural Science Foundation of Shandong Province of China

(ZR2018MB016), and the Young Taishan Scholars Program of Shandong Province (TSQN20161036).

Appendix A. Supplementary material

Experimental section and characterizations of **PI-0**, **PI-1**, **PI-2**, **Rh-1**, **Rh-2**, and **PI-Rh**, photostability of **PI-Rh**, optimum pH and response time of colorimetric fluorescent probe, HRMS spectrum of the response products, selectivity and interference experiments, analysis of the recovery of N_2H_4 and Hg^{2+} in actual samples, and **PI-Rh**–impregnated test paper for Hg^{2+} detection. Supplementary data to this article can be found online at https://doi.org/10.1016/j.saa.2021.119868.

References

[1] J.-W. Mo, B. Ogorevc, X. Zhang, B. Pihlar, Cobalt and copper hexacyanoferrate modified carbon fiber microelectrode as an all-solid potentiometric microsensor for hydrazine, Electroanalysis 12 (2000) 48–54, https://doi.org/10.1002/(SICI)1521-4109(20000101)12:1<48::AID-ELAN48>3.0.CO;2-H.

[2] I.C. Vieira, K.O. Lupetti, O. Fatibello-Filho, Sweet potato (ipomoea batatas (L.) Lam.) tissue as a biocatalyst in a paraffin/graphite biosensor for hydrazine determination in boiler feed water, Anal. Lett. 14 (2002) 2221–2231, https://doi.org/10.1081/AL-120016097.

[3] U. Ragnarsson, Synthetic methodology for alkyl substituted hydrazines, Chem. Soc. Rev. 30 (2001) 205–213, https://doi.org/10.1039/B010091A.

[4] A. Balsamo, B. Macchia, F. Macchia, A. Rossello, R. Giani, G. Pifferi, M. Pinza, G. Broccali, Synthesis and antibacterial activities of new (α-hydrazinobenzyl)cephalosporins, J. Med. Chem. 26 (1983) 1648–1650, https://doi.org/10.1021/jm00365a019.

[5] C.W. Huffman, E.M. Godar, K. Ohki, D.C. Torgeson, Synthesis of hydrazine derivatives as plant growth inhibitors, J. Agric. Food Chem. 16 (1968) 1041–1046, https://doi.org/10.1021/jf60160a035.

[6] W.C. Keller, Toxicity assessment of hydrazine fuels, Aviation Space Environ. Med. 59 (1988) A100–A106.

[7] S. Garrod, M.E. Bollard, A.W. Nicholls, S.C. Connor, J. Connelly, J.K. Nicholson, E. Holmes, Integrated metabonomic analysis of the multiorgan effects of hydrazine toxicity in the rat, Chem. Res. Toxicol. 18 (2005) 115–122, https://doi.org/10.1021/tx0498915.

[8] C.A. Reilly, S.D. Aust, Peroxidase substrates stimulate the oxidation of hydralazine to metabolites which cause single-strand breaks in DNA, Chem. Res. Toxicol. 10 (1997) 328–334, https://doi.org/10.1021/tx960189l.

[9] S.D. Zelnick, D.R. Mattie, Occupational exposure to hydrazines: treatment of acute central nervous system toxicity, Aviat. Space Environ. Med. 74 (2003) 1285–1291.

[10] Y.-Y. Liu, I. Schmeltz, D. Hoffmann, Chemical studies on tobacco smoke. Quantitative analysis of hydrazine in tobacco and cigarette smoke, Anal. Chem. 46 (1974) 885–889, https://doi.org/10.1021/ac60343a046.

[11] O. Gyllenhaal, L. Grönberg, J. Vessman, Determination of hydrazine in hydralazine by capillary gas chromatography with nitrogen-selective detection after benzaldehyde derivatization, J. Chromatogr. 511 (1990) 303–315, https://doi.org/10.1016/S0021-9673(01)93293-5.

[12] M. Sun, L. Bai, D.Q. Liu, A generic approach for the determination of trace hydrazine in drug substances using in situ derivatization-headspace GC-MS, J. Pharm. Biomed. Anal. 49 (2009) 529–533, https://doi.org/10.1016/j.jpba.2008.11.009.

[13] D.P. Elder, D. Snodin, A. Teasdale, Control and analysis of hydrazine, hydrazides and hydrazones-genotoxic impurities in active pharmaceutical ingredients (APIs) and drug products, J. Pharm. Biomed. Anal. 54 (2011) 900–910, https://doi.org/10.1016/j.jpba.2010.11.007.

[14] S.E.F. Kleijn, B. Serrano-Bou, A.I. Yanson, M.T.M. Koper, Influence of hydrazine-induced aggregation on the electrochemical detection of platinum nanoparticles, Langmuir 29 (2013) 2054–2064, https://doi.org/10.1021/la3040566.

[15] J. Liu, Y. Li, J. Jiang, X. Huang, C@ZnOnanorod array-based hydrazine electrochemical sensor with improved sensitivity and stability, Dalton Trans. 39 (2010) 8693–8697, https://doi.org/10.1039/C0DT00258E.

[16] H.E. Malone, Determination of mixtures of hydrazine and 1,1-dimethylhydrazine, Anal. Chem. 33 (1961) 575–577, https://doi.org/10.1021/ac60172a027.

[17] A. Umar, M.M. Rahman, S.H. Kim, Y.-B. Hahn, Zinc oxide nanonail based chemical sensor for hydrazine detection, Chem. Commun. 2 (2008) 166–168, https://doi.org/10.1039/B711215G.

[18] X. Gu, J.P. Camden, Surface-enhanced Raman spectroscopy-based approach for ultrasensitive and selective detection of hydrazine, Anal. Chem. 87 (2015) 6460–6464, https://doi.org/10.1021/acs.analchem.5b01566.

[19] X. Chen, Y. Xiang, Z. Li, A. Tong, Sensitive and selective fluorescence determination of trace hydrazine in aqueous solution utilizing 5-chlorosalicylaldehyde, Anal. Chim. Acta 625 (2008) 41–46, https://doi.org/10.1016/j.aca.2008.07.016.

[20] L. Xiao, J. Tu, S. Sun, Z. Pei, Y. Pei, Y. Pang, Y. Xu, A fluorescent probe for hydrazine and its in vivo applications, Rsc. Adv. 4 (2014) 41807–41811, https://doi.org/10.1039/C4RA08101C.

[21] Y. Zhang, Y. Huang, Y. Yue, J. Chao, F. Huo, C. Yin, A compact fluorescent probe based on *o*-phthalaldehyde for ultrasensitive detection of hydrazine in gas and solution phases, Sensor Actuat. B-Chem. 273 (2018) 944–950, https://doi.org/10.1016/j.snb.2018.06.112.

[22] J. Fan, W. Sun, M. Hu, J. Cao, G. Cheng, H. Dong, K. Song, Y. Liu, S. Sun, X. Peng, An ICT-based ratiometric probe for hydrazine and its application in live cells, Chem. Commun. 48 (2012) 8117–8119, https://doi.org/10.1039/C2CC34168A.

[23] Y. Tan, J. Yu, J. Gao, Y. Cui, Y. Yang, G. Qian, A new fluorescent and colorimetric probe for trace hydrazine with a wide detection range in aqueous solution, Dyes Pigm. 99 (2013) 966–971, https://doi.org/10.1016/j.dyepig.2013.08.008.

[24] M. Sun, J. Guo, Q. Yang, N. Xiao, Y. Li, A new fluorescent and colorimetric sensor for hydrazine and its application in biological systems, J. Mater. Chem. B 2 (2014) 1846–1851, https://doi.org/10.1039/C3TB21753A.

[25] B. Chen, X. Sun, X. Li, H. Ågren, Y. Xie, TICT based fluorescence "turn-on" hydrazine probes, Sensor Actuat. B-Chem. 199 (2014) 93–100, https://doi.org/10.1016/j.snb.2014.03.087.

[26] S. Sinha, P. Gaur, S. Dev, S. Mukhopadhyay, T. Mukherjee, S. Ghosh, Hydrazine responsive molecular material: optical signaling and mushroom cell staining, Sensor Actuat. B-Chem. 221 (2015) 418–426, https://doi.org/10.1016/j.snb.2015.06.100.

[27] S.I. Reja, N. Gupta, V. Bhalla, D. Kaur, S. Arora, M. Kumar, A charge transfer based ratiometric fluorescent probe for detection of hydrazine in aqueous medium and living cells, Sensor Actuat. B-Chem. 222 (2016) 923–929, https://doi.org/10.1016/j.snb.2015.08.078.

[28] J. Ma, J. Fan, H. Li, Q. Yao, J. Xia, J. Wang, X. Peng, Probing hydrazine with a near-infrared fluorescent chemodosimeter, Dyes Pigm. 138 (2017) 39–46, https://doi.org/10.1016/j.dyepig.2016.11.026.

[29] X. Yang, Y. Liu, Y. Wu, X. Ren, D. Zhang, Y. Ye, A NIR ratiometric probe for hydrazine "naked eye" detection and its imaging in living cell, Sensor Actuat. B-Chem. 253 (2017) 488–494, https://doi.org/10.1016/j.snb.2017.06.165.

[30] Z. Li, W. Zhang, C. Liu, M. Yu, H. Zhang, L. Guo, L. Wei, A colorimetric and ratiometric fluorescent probe for hydrazine and its application in living cells with low dark toxicity, Sensor Actuat. B-Chem. 241 (2017) 665–671, https://doi.org/10.1016/j.snb.2016.10.141.

[31] Y. Liu, D. Ren, J. Zhang, H. Li, X.-F. Yang, A fluorescent probe for hydrazine based on a newly developed 1-indanone-fused coumarin scaffold, Dyes Pigm. 162 (2019) 112–119, https://doi.org/10.1016/j.dyepig.2018.10.012.

[32] J. Wu, J. Pan, Z. Ye, L. Zeng, D. Su, A smart fluorescent probe for discriminative detection of hydrazine and bisulfite from different emission channels, Sensor Actuat. B-Chem. 274 (2018) 274–284, https://doi.org/10.1016/j.snb.2018.07.161.

[33] M.G. Choi, J. Hwang, J.O. Moon, J. Sung, S.-K. Chang, Hydrazine-selective chromogenic and fluorogenic probe based on levulinated coumarin, Org. Lett. 13 (2011) 5260–5263, https://doi.org/10.1021/ol202136q.

[34] S. Zhu, W. Lin, L. Yuan, Development of a near-infrared fluorescent probe for monitoring hydrazine in serum and living cells, Anal. Methods 5 (2013) 3450–3453, https://doi.org/10.1039/C3AY40540K.

[35] S. Goswami, S. Das, K. Aich, B. Pakhira, S. Panja, S.K. Mukherjee, S. Sarkar, A chemodosimeter for the ratiometric detection of hydrazine based on return of ESIPT and its application in live-cell imaging, Org. Lett. 15 (2013) 5412–5415, https://doi.org/10.1021/ol4026759.

[36] C. Hu, W. Sun, J. Cao, P. Gao, J. Wang, J. Fan, F. Song, S. Sun, X. Peng, A ratiometric near-infrared fluorescent probe for hydrazine and its in vivo applications, Org. Lett. 15 (2013) 4022–4025, https://doi.org/10.1021/ol401838p.

[37] B. Liu, Q. Liu, M. Shah, J. Wang, G. Zhang, Y. Pang, Fluorescence monitor of hydrazine in vivo by selective deprotection of flavonoid, Sensor Actuat. B-Chem. 202 (2014) 194–200, https://doi.org/10.1016/j.snb.2014.05.010.

[38] Y. Qian, J. Lin, L. Han, L. Lin, H. Zhu, A resorufin-based colorimetric and fluorescent probe for live-cell monitoring of hydrazine, Biosens. Bioelectron. 58 (2014) 282–286, https://doi.org/10.1016/j.bios.2014.02.059.

[39] J. Zhang, L. Ning, J. Liu, J. Wang, B. Yu, X. Liu, X. Yao, Z. Zhang, H. Zhang, Naked-eye and near-infrared fluorescence probe for hydrazine and its applications in in vitro and in vivo bioimaging, Anal. Chem. 87 (2015) 9101–9107, https://doi.org/10.1021/acs.analchem.5b02527.

[40] X. Jin, C. Liu, X. Wang, H. Huang, X. Zhang, H. Zhu, A flavone-based ESIPT fluorescent sensor for detection of N_2H_4 in aqueous solution and gas state and its imaging in living cells, Sensor Actuat. B-Chem. 216 (2015) 141–149, https://doi.org/10.1016/j.snb.2015.03.088.

[41] Y. Sun, D. Zhao, S. Fan, L. Duan, A 4-hydroxynaphthalimide-derived ratiometric fluorescent probe for hydrazine and its in vivo applications, Sensor Actuat. B-Chem. 208 (2015) 512–517, https://doi.org/10.1016/j.snb.2014.11.057.

[42] S. Yu, S. Wang, H. Yu, Y. Feng, S. Zhang, M. Zhu, H. Yin, X. Meng, A ratiometric two-photon fluorescent probe for hydrazine and its applications, Sensor Actuat. B-Chem. 220 (2015) 1338–1345, https://doi.org/10.1016/j.snb.2015.07.051.

[43] X. Xia, F. Zeng, P. Zhang, J. Lyu, Y. Huang, S. Wu, An ICT-based ratiometric fluorescent probe for hydrazine detection and its application in living cells and in vivo, Sensor Actuat. B-Chem. 227 (2016) 411–418, https://doi.org/10.1016/j.snb.2015.12.046.

[44] X. Zhang, C. Shi, P. Ji, X. Jin, J. Liu, H. Zhu, A red-emitting fluorescent probe based on flavone for hydrazine detection and its application in aqueous solution, Anal. Methods 8 (2016) 2267–2273, https://doi.org/10.1039/C5AY03313F.

[45] Z. Lu, W. Fan, X. Shi, Y. Lu, C. Fan, Two distinctly separated emission colorimetric NIR fluorescent probe for fast hydrazine detection in living cells and mice upon independent excitations, Anal. Chem. 89 (2017) 9918–9925, https://doi.org/10.1021/acs.analchem.7b02149.
[46] Y. Hao, Y. Zhang, K. Ruan, W. Chen, B. Zhou, X. Tan, Y. Wang, L. Zhao, G. Zhang, P. Qu, M. Xu, A naphthalimide-based chemodosimetric probe for ratiometric detection of hydrazine, Sensor Actuat. B-Chem. 244 (2017) 417–424, https://doi.org/10.1016/j.snb.2016.12.145.
[47] C. Liu, F. Wang, T. Xiao, B. Chi, Y. Wu, D. Zhu, X. Chen, The ESIPT fluorescent probes for N_2H_4 based on benzothiazol and their applications for gas sensing and bioimaging, Sensor Actuat. B-Chem. 256 (2018) 55–62, https://doi.org/10.1016/j.snb.2017.09.198.
[48] X. Shi, F. Huo, J. Chao, C. Yin, A ratiometric fluorescent probe for hydrazine based on novel cyclization mechanism and its application in living cells, Sensor Actuat. B-Chem. 260 (2018) 609–616, https://doi.org/10.1016/j.snb.2017.12.202.
[49] Z. Lu, X. Shi, Y. Ma, W. Fan, Y. Lu, Z. Wang, C. Fan, A simple two-output near-infrared fluorescent probe for hydrazine detection in living cells and mice, Sensor Actuat. B-Chem. 258 (2018) 42–49, https://doi.org/10.1016/j.snb.2017.11.125.
[50] S. Wang, S. Ma, J. Zhang, M. She, P. Liu, S. Zhang, J. Li, A highly sensitive and selective near-infrared fluorescent probe for imaging hydrazine in living tissues and mice, Sensor Actuat. B-Chem. 261 (2018) 418–424, https://doi.org/10.1016/j.snb.2018.01.126.
[51] L. Cui, C. Ji, Z. Peng, L. Zhong, C. Zhou, L. Yan, S. Qu, S. Zhang, C. Huang, X. Qian, Y. Xu, Unique tri-output optical probe for specific and ultrasensitive detection of hydrazine, Anal. Chem. 86 (2014) 4611–4617, https://doi.org/10.1021/ac5007552.
[52] L. Cui, Z. Peng, C. Ji, J. Huang, D. Huang, J. Ma, S. Zhang, X. Qian, Y. Xu, Hydrazine detection in the gas state and aqueous solution based on the Gabriel mechanism and its imaging in living cells, Chem. Commun. 50 (2014) 1485–1487, https://doi.org/10.1039/C3CC48304E.
[53] F. Ali, H.A. Anila, N. Taye, D.G. Mogare, S. Chattopadhyay, A. Das, Specific receptor for hydrazine: mapping the in situ release of hydrazine in live cells and in an in vitro enzymatic assay, Chem. Commun. 52 (2016) 6166–6169, https://doi.org/10.1039/C6CC01787H.
[54] B. Li, Z. He, H. Zhou, H. Zhang, W. Li, T. Cheng, G. Liu, Reaction based colorimetric and fluorescence probes for selective detection of hydrazine, Dyes Pigm. 146 (2017) 300–304, https://doi.org/10.1016/j.dyepig.2017.07.023.
[55] B. Shi, Y. He, P. Zhang, Y. Wang, M. Yu, H. Zhang, L. Wei, Z. Li, Turn on fluorescent detection of hydrazine with a 1,8-naphthalimde derivative, Dyes Pigm. 147 (2017) 152–159, https://doi.org/10.1016/j.dyepig.2017.08.010.
[56] M.V.R. Raju, E.C. Prakash, H.-C. Chang, H.-C. Lin, A facile ratiometric fluorescent chemodosimeter for hydrazine based on Ing-Manske hydrazinolysis and its applications in living cells, Dyes Pigm. 103 (2014) 9–20, https://doi.org/10.1016/j.dyepig.2013.11.015.
[57] W.-D. Wang, Y. Hu, Q. Li, S.-L. Hu, A carbazole-based turn-on fluorescent probe for the detection of hydrazine in aqueous solution, Inorg. Chim. Acta 477 (2018) 206–211, https://doi.org/10.1016/j.ica.2018.03.033.
[58] L. Wang, F. Liu, H. Liu, Y.D.T. Liu, J. Liu, Y. Yao, X. Wan, A novel pyrazoline-based fluorescent probe for detection of hydrazine in aqueous solution and gas state and its imaging in living cells, Sensor Actuat. B-Chem. 229 (2016) 441–452, https://doi.org/10.1016/j.snb.2016.02.001.
[59] M.H. Lee, B. Yoon, J.S. Kim, J.L. Sessler, Naphthalimide trifluoroacetyl acetonate: a hydrazine-selective chemodosimetric sensor, Chem. Sci. 4 (2013) 4121–4126, https://doi.org/10.1039/C3SC51813B.
[60] B. Roy, S. Halder, A. Guha, S. Bandyopadhyay, Highly selective sub-ppm naked-eye detection of hydrazine with conjugated-1,3-diketo probes: imaging hydrazine in drosophila larvae, Anal. Chem. 89 (2017) 10625–10636, https://doi.org/10.1021/acs.analchem.7b03503.
[61] Z. Luo, B. Liu, T. Qin, K. Zhu, C. Zhao, C. Zhao, C. Pan, L. Wang, Cyclization of chalcone enables ratiometric fluorescence determination of hydrazine with a high selectivity, Sensor Actuat. B-Chem. 263 (2018) 229–236, https://doi.org/10.1016/j.snb.2018.02.120.
[62] H. Xu, B. Gu, Y. Li, Z. Huang, W. Su, X. Duan, P. Yin, H. Li, S. Yao, A highly selective, colorimetric and ratiometric fluorescent probe for NH_2NH_2 and its bioimaging, Talanta 180 (2018) 199–205, https://doi.org/10.1016/j.talanta.2017.12.039.
[63] (a) B. Zhu, X. Wu, J. Rodrigues, X. Hu, R. Sheng, G.-M. Bao, A dual-analytes responsive fluorescent probe for discriminative detection of ClO- and N2H4 in living cells, Spectrochim. Acta A 246 (2021), https://doi.org/10.1016/j.saa.2020.118953 118953;
(b) L. Jiang, Q. Hu, T. Chen, D. Min, H.-Q. Yuan, G.-M. Bao, Highly sensitive and rapid responsive fluorescence probe for determination of formaldehyde in seafood and in vivo imaging application, Spectrochim. Acta A 228 (2020), https://doi.org/10.1016/j.saa.2019.117789 117789.
[64] M.F. Wolfe, S. Schwarzbach, R.A. Sulaiman, Effects of mercury on wildlife: A comprehensive review, Environ. Toxicol. Chem. 17 (1998) 146–160, https://doi.org/10.1002/etc.5620170203.
[65] E.K. Silbergeld, I.A. Silva, J.F. Nyland, Mercury and autoimmunity: implications for occupational and environmental health, Toxicol. Appl. Pharmacol. 207 (2005) 282–292, https://doi.org/10.1016/j.taap.2004.11.035.
[66] X. Chen, T. Pradhan, F. Wang, J.S. Kim, J. Yoon, Fluorescent chemosensors based on spiroring-opening of xanthenes and related derivatives, Chem. Rev. 112 (2012) 1910–1956, https://doi.org/10.1021/cr200201z.
[67] H.N. Kim, W.X. Ren, J.S. Kim, J. Yoon, Fluorescent and colorimetric sensors for detection of lead, cadmium, and mercury ions, Chem. Soc. Rev. 41 (2012) 3210–3244, https://doi.org/10.1039/C1CS15245A.
[68] H. Zheng, X.-Q. Zhan, Q.-N. Biana, X.-J. Zhang, Advances in modifying fluorescein and rhodamine fluorophores as fluorescent chemosensors, Chem. Commun. 49 (2013) 429–447, https://doi.org/10.1039/C2CC35997A.
[69] J. Fan, M. Hu, P. Zhan, X. Peng, Energy transfer cassettes based on organic fluorophores: construction and applications in ratiometric sensing, Chem. Soc. Rev. 42 (2013) 29–43, https://doi.org/10.1039/C2CS35273G.
[70] K.P. Carter, A.M. Young, A.E. Palmer, Fluorescent sensors for measuring m1etal ions in living systems, Chem. Rev. 114 (2014) 4564–4601, https://doi.org/10.1021/cr400546e.
[71] X. Qian, Z. Xu, Fluorescence imaging of metal ions implicated in diseases, Chem. Soc. Rev. 44 (2015) 4487–4493, https://doi.org/10.1039/C4CS00292J.
[72] Y. Chen, W. Zhang, Y. Cai, R.T.K. Kwok, Y. Hu, J.W.Y. Lam, X. Gu, Z. He, Z. Zhao, X. Zheng, B. Chen, C. Gui, B.Z. Tang, AIEgens for dark through-bond energy transfer: design, synthesis, theoretical study and application in ratiometric Hg^{2+} sensing, Chem. Sci. 8 (2017) 2047–2055, https://doi.org/10.1039/C6SC04206F.
[73] M. Wang, J. Wen, Z. Qin, H. Wang, A new coumarin–rhodamine FRET system as an efficient ratiometric fluorescent probe for Hg^{2+} in aqueous solution and in living cells, Dyes Pigm. 120 (2015) 208–212, https://doi.org/10.1016/j.dyepig.2015.04.013.
[74] F.-H. Wang, C.-W. Cheng, L.-C. Duan, W. Lei, M.-Z. Xia, F.-Y. Wang, Highly selective fluorescent sensor for Hg^{2+} ion based on a novel rhodamine B derivative, Sensor Actuat. B-Chem. 206 (2015) 679–683, https://doi.org/10.1016/j.snb.2014.10.008.
[75] Y.-X. Wu, X.-B. Zhang, D.-L. Zhang, C.-C. Zhang, J.-B. Li, Y. Wu, Z.-L. Song, R.-Q. Yu, W. Tan, Quench-shield ratiometric upconversion luminescence nanoplatform for biosensing, Anal. Chem. 88 (2016) 1639–1646, https://doi.org/10.1021/acs.analchem.5b03573.
[76] Y. Ge, X. Xing, A. Liu, R. Ji, S. Shen, X. Cao, A novel imidazo[1,5-a]pyridine-rhodamine FRET system as an efficient ratiometric fluorescent probe for Hg^{2+} in living cells, Dyes Pigm. 146 (2017) 136–142, https://doi.org/10.1016/j.dyepig.2017.06.067.
[77] G. Singh, S.I. Reja, V. Bhalla, D. Kaur, P. Kaur, S. Arora, M. Kumar, Hexaphenylbenzene appended AIEE active FRET based fluorescent probe for selective imaging of Hg^{2+} ions in MCF-7 cell lines, Sensor Actuat. B-Chem. 249 (2017) 311–320, https://doi.org/10.1016/j.snb.2017.04.074.
[78] Y. Ge, A. Liu, R. Ji, S. Shen, X. Cao, Detection of Hg^{2+} by a FRET ratiometric fluorescent probe based on a novel pyrido[1,2-a]benzimidazole-rhodamine system, Sensor Actuat. B-Chem. 251 (2017) 410–415, https://doi.org/10.1016/j.snb.2017.05.097.
[79] X. Yang, X. Qin, Y. Li, M. Yan, Y. Cui, G. Sun, TBET-based ratiometric fluorescent probe for Hg^{2+} with large pseudo-Stokes shift and emission shift in aqueous media and intracellular colorimetric imaging in live Hela cells, Biosens. Bioelectron. 121 (2018) 62–71, https://doi.org/10.1016/j.bios.2018.09.004.
[80] Y. Fang, X. Li, J.-Y. Li, G.-Y. Wang, Y. Zhou, N.-Z. Xu, Y. Hu, C. Yao, Thiooxo-Rhodamine B hydrazone derivatives bearing bithiophene group as fluorescent chemosensors for detecting mercury(II) in aqueous media and living HeLa cells, Sensor Actuat. B-Chem. 255 (2018) 1182–1190, https://doi.org/10.1016/j.snb.2017.06.050.
[81] M. Santra, B. Roy, K.H. Ahn, A "reactive" ratiometric fluorescent probe for mercury species, Org. Lett. 13 (2011) 3422–3425, https://doi.org/10.1021/ol2011693.
[82] W. Gong, B. Gao, J. Zhao, G. Ning, Rational design of a reusable chemodosimeter for the selective detection of Hg^{2+}, J. Mater. Chem. A 1 (2013) 5501–5504, https://doi.org/10.1039/C3TA10412E.
[83] H. Jiang, J. Jiang, J. Cheng, W. Dou, X. Tang, L. Yang, W. Liu, D. Bai, A sensitive colorimetric and ratiometric fluorescent chemodosimeter for Hg^{2+} and its application for bioimaging, New J. Chem. 38 (2014) 109–114, https://doi.org/10.1039/C3NJ00766A.
[84] Y. Han, C. Yang, K. Wu, Y. Chen, B. Zhou, M. Xia, A facile naphthalene-based fluorescent chemodosimeter for mercury ions in aqueous solution, RSC Adv. 5 (2015) 16723–16726, https://doi.org/10.1039/C4RA16479B.
[85] X. Shang, N. Wang, R. Cerny, W. Niu, J. Guo, Fluorescent protein-based "turn-on" probe through a general protection-deprotection design strategy, ACS Sens. 2 (2017) 961–966, https://doi.org/10.1021/acssensors.7b00223.
[86] W. Jiang, W. Wang, A selective and sensitive "turn-on" fluorescent chemodosimeter for Hg^{2+} in aqueous media via Hg^{2+} promoted facile desulfurization-lactonization reaction, Chem. Commun. 26 (2009) 3913–3915, https://doi.org/10.1039/B903606G.
[87] W. Xuan, C. Chen, Y. Cao, W. He, W. Jiang, K. Liu, W. Wang, Rational design of a ratiometric fluorescent probe with a large emission shift for the facile detection of Hg^{2+}, Chem. Commun. 48 (2012) 7292–7294, https://doi.org/10.1039/C2CC32435K.
[88] W. Shu, L. Yan, J. Liu, Z. Wang, S. Zhang, C. Tang, C. Liu, B. Zhu, B. Du, Highly selective fluorescent probe for the sensitive detection of inorganic and organic mercury species assisted by H_2O_2, Ind. Eng. Chem. Res. 54 (2015) 8056–8062, https://doi.org/10.1021/acs.iecr.5b02153.
[89] W. Shu, Y. Wang, L. Wu, Z. Wang, Q. Duan, Y. Gao, C. Liu, B. Zhu, L. Yan, A novel carbonothioate-based colorimetric and fluorescent probe for selective detection of mercury ions, Ind. Eng. Chem. Res. 55 (2016) 8713–8718, https://doi.org/10.1021/acs.iecr.6b02158.

[90] A.S. Rao, D. Kim, T. Wang, K.H. Kim, S. Hwang, K.H. Ahn, Reaction-based two-photon probes for mercury ions: fluorescence imaging with dual optical windows, Org. Lett. 14 (2012) 2598–2601, https://doi.org/10.1021/ol3009057.
[91] J. Ding, H. Li, C. Wang, J. Yang, Y. Xie, Q. Peng, Q. Li, Z. Li, "Turn-on" fluorescent probe for mercury(II):high selectivity and sensitivity and new design approach by the adjustment of the π-bridge, ACS Appl. Mater. Interfaces 7 (2015) 11369–11376, https://doi.org/10.1021/acsami.5b01800.
[92] J. Ding, H. Li, Y. Xie, Q. Peng, Q. Li, Z. Li, Reaction-based conjugated polymer fluorescent probe for mercury(II):good sensing performance with "turn-on" signal output, Polym. Chem. 8 (2017) 222l–2226l, https://doi.org/10.1039/C7PY00035A.
[93] Z. Zhang, B. Zhang, X. Qian, Z. Li, Z. Xu, Y. Yang, Simultaneous quantification of Hg^{2+} and $MeHg^{+}$ in aqueous media with a single fluorescent probe by multiplexing in the time domain, Anal. Chem. 86 (2014) 11919–11924, https://doi.org/10.1021/ac503900w.
[94] J. Liu, Y.-Q. Sun, P. Wang, J. Zhang, W. Guo, Construction of NIR and ratiometric fluorescent probe for Hg^{2+} based on a rhodamine-inspired dye platform, Analyst 138 (2013) 2654–2660, https://doi.org/10.1039/C3AN00061C.
[95] X. Yang, Y. Li, Y. Ding, Z. Zhao, Y. Zhang, X. Liu, Z. Fu, Y. Cui, G. Sun, G. Zhang, M. Yan, Ratiometric & reversible fluorescent sensing of NaCN by an effective probe based on phenanthro[9,10-d]imidazole platform, Sensor Actuat. B-Chem. 253 (2017) 478–487, https://doi.org/10.1016/j.snb.2017.05.186.
[96] W. Lin, L. Long, L. Yuan, Z. Cao, B. Chen, W. Tan, A ratiometric fluorescent probe for cysteine and homocysteine displaying a large emission shift, Org. Lett. 10 (2008) 5577–5580, https://doi.org/10.1021/ol802436j.
[97] M.J. Frisch, G.W. Trucks, H.B. Schlegel, G.E. Scuseria, M.A. Robb, J.R. Cheeseman, J.A. Montgomery Jr., T. Vreven, K.N. Kudin, J.C. Burant, J.M. Millam, S. S. Iyengar, J. Tomasi, V. Barone, B. Mennucci, M. Cossi, G. Scalmani, N. Rega, G.A. Petersson, H. Nakatsuji, M. Hada, M. Ehara, K. Toyota, R. Fukuda, J. Hasegawa, M. Ishida, T. Nakajima, Y. Honda, O. Kitao, H. Nakai, M. Klene, X. Li, J.E. Knox, H. P. Hratchian, J.B. Cross, V. Bakken, C. Adamo, J. Jaramillo, R. Gomperts, R.E. Stratmann, O. Yazyev, A.J. Austin, R. Cammi, C. Pomelli, J.W. Ochterski, P.Y. Ayala, K. Morokuma, G.A. Voth, P. Salvador, J.J. Dannenberg, V.G. Zakr-zewski, S. Dapprich, A.D. Daniels, M.C. Strain, O. Farkas, D.K. Malick, A.D. Rabuck, K. Raghavachari, J.B. Foresman, J.V. Ortiz, Q. Cui, A.G. Baboul, S. Clifford, J. Cioslowski, B.B. Stefanov, G. Liu, A. Liashenko, P. Piskorz, I. Komaromi, R.L. Martin, D.J. Fox, T. Keith, M.A. Al-Laham, C.Y. Peng, A. Nanayakkara, M. Challacombe, P.M. W. Gill, B. Johnson, W. Chen, M.W. Wong, C. Gonzalez, J.A. Pople, Gaussian 03, Revision C02, 2004, Gaussian Inc., Pittsburgh, PA.